

Patterns in Wall-Bounded Shear Flows

Laurette S. Tuckerman,¹ Matthew Chantry,²
and Dwight Barkley³

¹Laboratoire de Physique et Mécanique des Milieux Hétérogènes (PMMH), CNRS UMR 7636, ESPCI Paris, PSL University, Sorbonne Université, and Université de Paris, Paris 75005, France; email: laurette@pmmh.espci.fr

²Atmospheric, Oceanic and Planetary Physics Research Group, University of Oxford, Oxford OX1 3PU, United Kingdom

³Mathematics Institute, University of Warwick, Coventry CV4 7AL, United Kingdom

Annu. Rev. Fluid Mech. 2020. 52:343–67

First published as a Review in Advance on
August 20, 2019

The *Annual Review of Fluid Mechanics* is online at
fluid.annualreviews.org

<https://doi.org/10.1146/annurev-fluid-010719-060221>

Copyright © 2020 by Annual Reviews.
All rights reserved

Keywords

transition to turbulence, wall-bounded shear flows, turbulent–laminar pattern, directed percolation

Abstract

Experiments and numerical simulations have shown that turbulence in transitional wall-bounded shear flows frequently takes the form of long oblique bands if the domains are sufficiently large to accommodate them. These turbulent bands have been observed in plane Couette flow, plane Poiseuille flow, counter-rotating Taylor–Couette flow, torsional Couette flow, and annular pipe flow. At their upper Reynolds number threshold, laminar regions carve out gaps in otherwise uniform turbulence, ultimately forming regular turbulent–laminar patterns with a large spatial wavelength. At the lower threshold, isolated turbulent bands sparsely populate otherwise laminar domains, and complete laminarization takes place via their disappearance. We review results for plane Couette flow, plane Poiseuille flow, and free-slip Waleffe flow, focusing on thresholds, wavelengths, and mean flows, with many of the results coming from numerical simulations in tilted rectangular domains that form the minimal flow unit for the turbulent–laminar bands.

ANNUAL
REVIEWS **CONNECT**

www.annualreviews.org

- Download figures
- Navigate cited references
- Keyword search
- Explore related articles
- Share via email or social media

1. INTRODUCTION

The transition to turbulence in wall-bounded shear flows is often said to be subcritical, which calls to mind the famous quotation by Stanislaw Ulam (Campbell et al. 1985, p. 374), “Using a term like nonlinear science is like referring to the bulk of zoology as the study of nonelephant animals.” An essential feature of transitional turbulence is its spatial inhomogeneity, also called spatial intermittency. Classical transitions in configurations such as corotating Taylor–Couette flow or Rayleigh–Bénard convection occur uniformly. There exists a threshold Reynolds number (Re) or Rayleigh number above which the laminar flow is linearly unstable and, after a relatively short time, the entire flow is occupied by a new state. For the wall-bounded shear flows that we describe, this is not true. All of these flows are linearly stable in the Reynolds number regime in which transition to turbulence occurs. For transition to take place, the flows must be subjected to a finite-amplitude perturbation. There are various critical Reynolds numbers, one below which the asymptotic state is uniform laminar flow, and another above which it is uniform turbulence, separated by an intermediate range in which the asymptotic state is a mixture, more or less organized, of laminar and turbulent flow. The flows in this intermediate range are the subject of this review.

2. PLANE COUETTE FLOW: TURBULENT-LAMINAR BANDED PATTERNS

Plane Couette flow is the flow between two parallel rigid plates that are separated by a fixed distance and that move at equal and opposite velocities. A particularly striking manifestation of spatial inhomogeneity in this system is a state consisting of persistent turbulent bands coexisting with nearly laminar regions, as shown in **Figure 1a**. **Supplemental Video 1** shows the emergence of a banded-turbulent pattern from uniform turbulence as Re decreases.

Such states occur in other similar shear flows. In particular, they occur in counter-rotating Taylor–Couette flow, the flow between concentric cylinders that rotate in opposite directions. Indeed, it was in counter-rotating Taylor–Couette flow that an oblique turbulent band—or in this geometry, a turbulent spiral—was first observed by Coles & van Atta (1966), as seen in **Figure 1b**.

Supplemental Material >

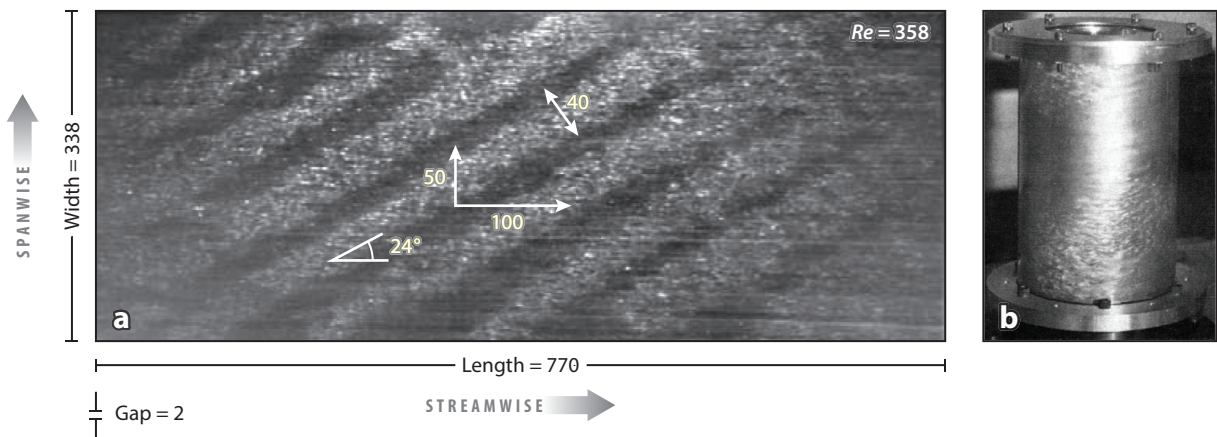


Figure 1

(a) Turbulent-laminar pattern in a plane Couette flow experiment at a Reynolds number (Re) of 358. All lengths are in units of the half-gap, b . (b) Turbulent spiral in a Taylor–Couette flow experiment. Panels adapted with permission from (a) Prigent et al. (2003) and (b) Coles & van Atta (1966).

This state was famously mentioned by Feynman (1964), and another depiction of it is included in the widely cited encyclopedic survey of Taylor–Couette flow by Andereck et al. (1986). (Because a translating frame is equivalent to a stationary one, only the relative velocity is significant in plane Couette flow. However, both relative and mean rotation are significant in Taylor–Couette flow. Consequently, flows with corotating and counter-rotating cylinders have quite different properties. In particular, a classic supercritical bifurcation occurs in parts of the corotating parameter space, while parts of the counter-rotating parameter space resemble plane Couette flow.)

Starting in the 1990s, it was shown that in a less confined geometry, the turbulent spiral is part of a regular alternating pattern that, moreover, also occurs in plane Couette flow. Tillmark & Alfredsson (1992) used a looped belt to conduct pioneering experiments on transition in plane Couette flow. Using a similar device, Daviaud et al. (1992) showed that turbulent spots grew into inclined patches and suggested that these might be related to the turbulent Taylor–Couette spirals. Prigent et al. (2002) then carried out experiments with large aspect ratios, i.e., spanwise and streamwise directions that were 338 and 770 times the half-gap between the plates for plane Couette flow and axial and azimuthal directions of 884 and 724 times the half-gap for counter-rotating Taylor–Couette flow. These large aspect ratios are necessary because the pattern wavelength is on the order of 40 times the half-gap. The bands are aligned obliquely (on the order of 24°) with respect to the streamwise direction. Both the wavelength and the angle depend, weakly but reproducibly, on the Reynolds numbers. This state can thus be called a turbulent–laminar banded pattern, and it has been studied extensively since then.

Turbulent–laminar banded patterns were first simulated numerically by Barkley & Tuckerman (2005a). A visualization of this pattern is shown in **Figure 2a** via the kinetic energy at mid-gap. While the turbulent bands are oriented obliquely to the streamwise direction, within each turbulent region are structures primarily aligned with the streamwise direction. These structures correspond to the streamwise vortices and streaks known to be the essential building blocks of

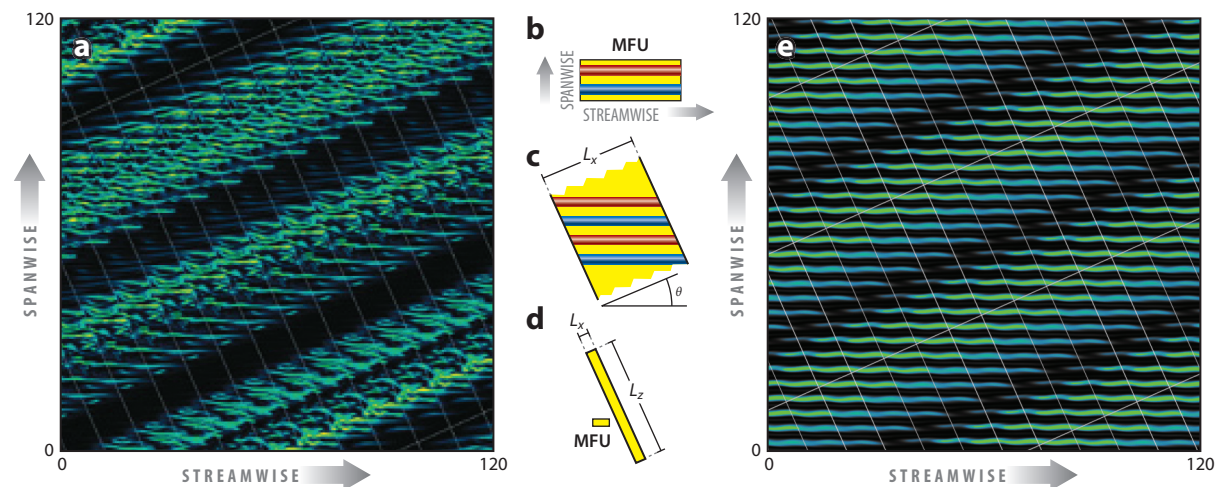


Figure 2

(a) A turbulent–laminar pattern for plane Couette flow at a Reynolds number of 350, calculated in a narrow rectangular tilted box. Shown is an instantaneous snapshot of the kinetic energy at mid-gap. The laminar regions are uniformly black, while the turbulent regions consist of narrow horizontal streaks and vortices. (b–d) The tilted box used for simulations. (e) The oblique unstable equilibrium state computed in a tilted domain by Reetz et al. (2019). All lengths are in units of the half-gap, *b*. Abbreviation: MFU, minimal flow unit. Panels *a* and *e* adapted with permission from Barkley & Tuckerman (2005a) and Reetz et al. (2019), respectively.

transitional shear turbulence (Hamilton et al. 1995, Waleffe 1997). The spanwise width of these structures is on the scale of the fluid gap. Streaks are clearly visible in **Supplemental Video 1**, which shows the streamwise velocity at the midplane.

A key feature of these simulations is the use of a periodic rectangular tilted domain, whose long direction is perpendicular to the bands, i.e., parallel to the wave vector of the pattern. Plates situated at $y = \pm b$ move at speed U in equal and opposite directions at an angle θ from the x axis. The laminar flow and Reynolds numbers are

$$\mathbf{u}_{\text{Cou}}^{\text{lam}} = U \frac{y}{b} \mathbf{e}_{\text{strm}} \equiv U \frac{y}{b} (\cos \theta \mathbf{e}_x + \sin \theta \mathbf{e}_z), \quad Re = Re_{\text{Cou}} \equiv \frac{Ub}{\nu}. \quad 1.$$

For $\theta = 0$, there is no tilt and Equation 1 reduces to the usual convention for plane Couette flow, $\mathbf{e}_{\text{strm}} = \mathbf{e}_x$. We call y the vertical or wall-normal direction and (x, z) the horizontal directions. Coordinates x and z here refer to the band-parallel and band-perpendicular directions; the streamwise and spanwise directions are referred to as such. Velocity components $\mathbf{u} \equiv (u, v, w)$ are specified where necessary. Where not otherwise specified, we use nondimensionalized variables such that $U = b = 1$ and Re refers to Re_{Cou} .

Figure 2b–d shows the construction principle for this domain. The idealized minimal flow unit (Hamilton et al. 1995) of size $[L_x, L_y, L_z] = [4, 2, 6]$ is shown in **Figure 2b**. There is no tilt and its spanwise width, $L_z = 4$, is such as to contain just one pair of counter-rotating streamwise vortices. (The nominal spanwise width of a single vortex is the size of the fluid gap, which in nondimensional units is 2.) In order to sensibly impose periodicity in a tilted domain, streamwise vortices must meet adjacent ones in crossing a boundary, as illustrated in **Figure 2c**. To maintain a vortex-pair spacing of approximately 4, the short direction of the domain L_x must be related to the angle θ by $L_x \approx 4 / \sin \theta$. **Figure 2c** shows a typical value of 24° for which we take $L_x = 10 \simeq 4 / \sin \theta = 9.83$. Finally, the remaining horizontal dimension L_z of the domain is taken to be long so as to contain one wavelength of the turbulent–laminar pattern, typically 40 half-gaps. This domain can be called the minimal band unit (MBU). The domain can also be prolonged, as in **Figure 2d**, to contain several repetitions of the pattern. The outlines of these domains, repeated periodically so as to tile **Figure 2a**, are seen as faint white lines.

Simulating turbulent–laminar patterns in tilted computational domains with a single long direction has two purposes. The first is the obvious reduction in the computational resources required compared to those for domains with two large directions. The second is that such simulations capture the minimal, or near-minimal, conditions necessary for turbulent–laminar patterns to form, and this allows more direct access to the mechanisms underlying these patterns.

Figure 2e shows an unstable equilibrium solution computed by Reetz et al. (2019) that greatly resembles the instantaneous pattern in **Figure 2a**. Following the first calculation of a nontrivial equilibrium by Nagata (1990), a large number of unstable equilibria (called exact coherent structures in the context of wall-bounded shear flows) have been computed (e.g., Gibson et al. 2009). The scenario deduced by Reetz et al. (2019) shows that the equilibrium in **Figure 2e** is connected to the Nagata solution via two successive bifurcations. Oblique equilibria have also been calculated by high- Re asymptotic methods by Deguchi & Hall (2015). Unstable equilibria are thought to play an underlying role in organizing turbulence (Cvitanović & Eckhardt 1989, Kawahara & Kida 2001). Schneider et al. (2010) have extended these ideas to compute edge states that are spatially localized within large domains and mildly chaotic. We do not focus further on equilibria; readers are referred to Kawahara et al. (2012).

Domains large in both the streamwise and spanwise directions, while less economical, can capture further features of the systems, such as competition between different angles and wavelengths. **Figure 3** shows turbulent–laminar banded patterns with competing angles in plane Couette flow

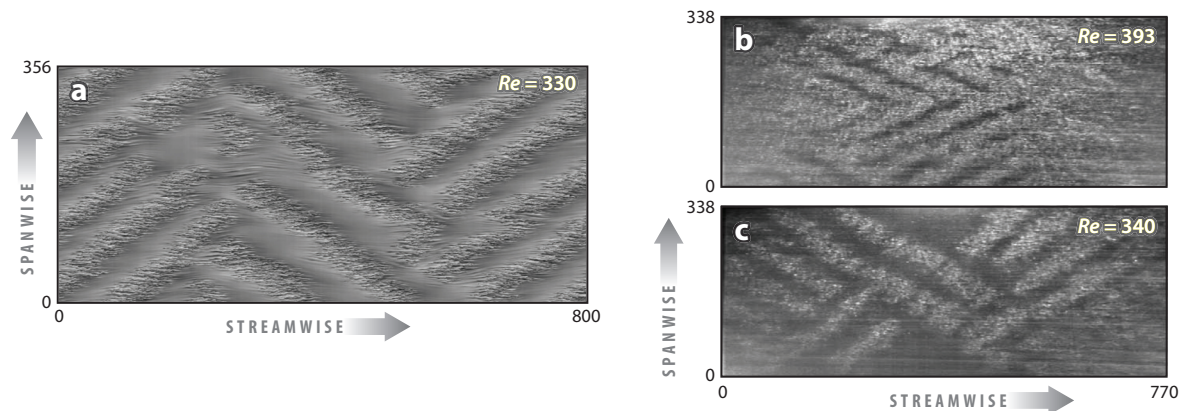


Figure 3

Competition in plane Couette flow between turbulent–laminar bands with opposite angles. (a) Streamwise velocity in midplane computed by Duguet et al. (2010) in a domain oriented along the streamwise and spanwise directions. (b,c) Plane Couette experiment of Prigent et al. (2003). The wavelength increases as Reynolds number (Re) decreases. All lengths are in units of the half-gap, b . Panels adapted with permission from (a) Duguet et al. (2010) and (b,c) Prigent et al. (2003).

from simulations by Duguet et al. (2010) and from experiments by Prigent et al. (2003). The competition between bands at opposite angles was studied by these authors and by Hegseth et al. (1989) and Goharzadeh & Mutabazi (2001, 2008) in terms of diffusive phase dynamics and Ginzburg–Landau equations.

Most of the simulations presented in this section were obtained using the spectral element/Fourier code `Prism` (Henderson & Karniadakis 1995) to integrate the Navier–Stokes equations on grids containing 6–12 points per unit length in the horizontal directions and 15–20 in the wall-normal direction in a domain tilted at 24° . We also present some simulations in large domains whose sides are aligned with the streamwise and spanwise directions.

Turbulent–laminar patterns are associated with large-scale and reproducible mean flows, as can be expected since they break the spatial homogeneity in the streamwise and spanwise directions. Entitling their article “Progress Report on a Digital Experiment in Spiral Turbulence” to highlight their then-groundbreaking experimental techniques, Coles & van Atta (1966) sketched the form of the mean flow at mid-gap between the two cylinders in their Taylor–Couette apparatus (**Figure 4a**). Results in **Figure 4b** from our full numerical computations in plane Couette flow show the mean flow to be somewhat different but also emphasize the importance of strong flow parallel to the band boundaries. Duguet & Schlatter (2013) showed that this along-band flow is a simple consequence of the incompressibility of the large-scale flow.

A more complete view of the mean structure of a turbulent–laminar pattern is presented in **Figure 5**. We use $\langle \cdot \rangle$ to denote averaging in time and along the band direction x , yielding functions that depend on the wall-normal direction y and the band-perpendicular direction z . The deviation from laminar Couette flow is plotted in a periodically prolonged domain. The centers of two adjacent turbulent bands are located at $z = -20$ and $z = 20$, as seen in the turbulent kinetic energy, E_{turb} . The intervening laminar region is centered on $z = 0$. The topmost plot shows the along-band flow $\langle u \rangle$ (into and out of the plane shown), which is strong at the interfaces. The flow along the bands is accompanied by a large-scale circulation around the turbulent bands, although we emphasize that this streamfunction $\langle \psi \rangle$ corresponds to the deviation from laminar Couette flow. For this periodic pattern, the mean flow can be approximated to high accuracy as the sum of only

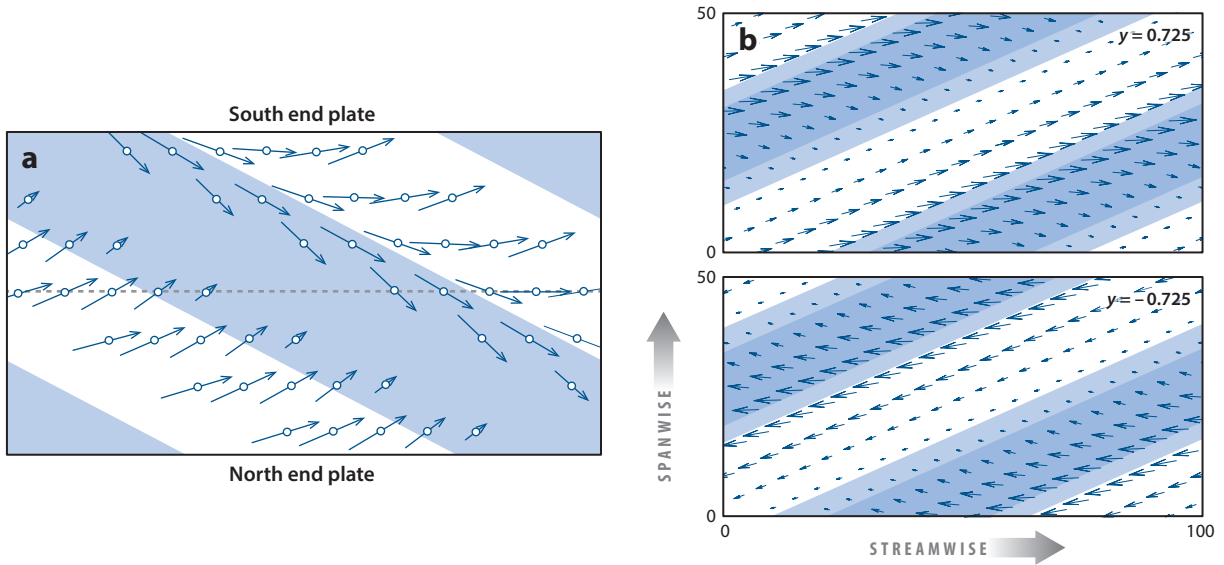


Figure 4

Horizontal views of flow accompanying the turbulent–laminar banded pattern. (a) Sketch from experimental data at midplane of Taylor–Couette flow (Coles & van Atta 1966). (b) Computations of plane Couette flow, above and below midplane. Turbulent regions are shown in blue and laminar regions are shown in white. Both show prominent band-parallel flow at the turbulent–laminar boundaries. All lengths are in units of the half-gap, *b*. Panels adapted with permission from (a) Coles & van Atta (1966) and (b) Barkley & Tuckerman (2007).

three trigonometric functions in the band-perpendicular direction z ,

$$u(y, z) \approx u_0(y) + u_c(y) \cos(2\pi z/\lambda) + u_s(y) \sin(2\pi z/\lambda), \quad 2.$$

where λ is the wavelength, here 40 half-gaps, and u represents $\langle u \rangle$ or $\langle \psi \rangle$.

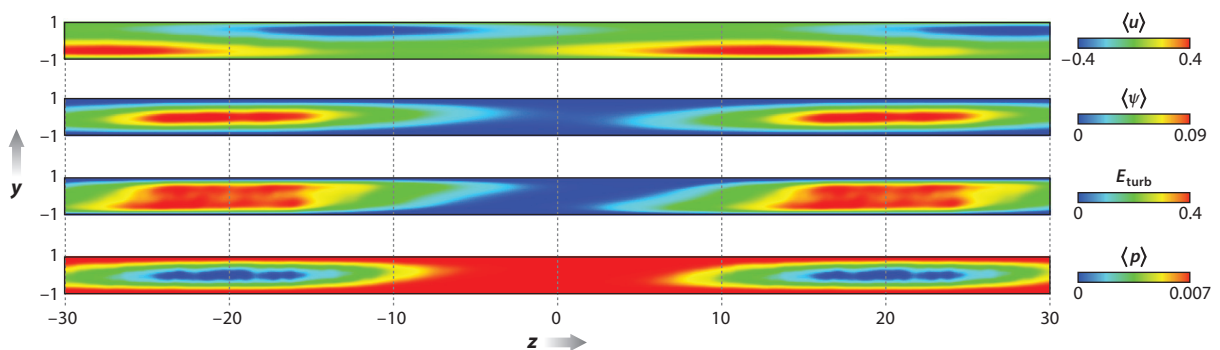


Figure 5

Mean flow of a turbulent–laminar pattern at a Reynolds number of 350, with the average taken over time and the band-parallel direction, and laminar plane Couette flow subtracted. The center of the turbulent bands is at $z = \pm 20$, the center of the laminar region is at $z = 0$, and the boundaries are at $z \approx \pm 10$. The band-parallel flow $\langle u \rangle$ is strongest at the boundaries. The flow in the (y, z) plane is represented by a streamfunction $\langle \psi \rangle$, which shows circulation around the turbulent band, characterized by high turbulent kinetic energy E_{turb} and low pressure $\langle p \rangle$. All lengths are in units of the half-gap, *b*. Figure adapted with permission from Barkley & Tuckerman (2007).

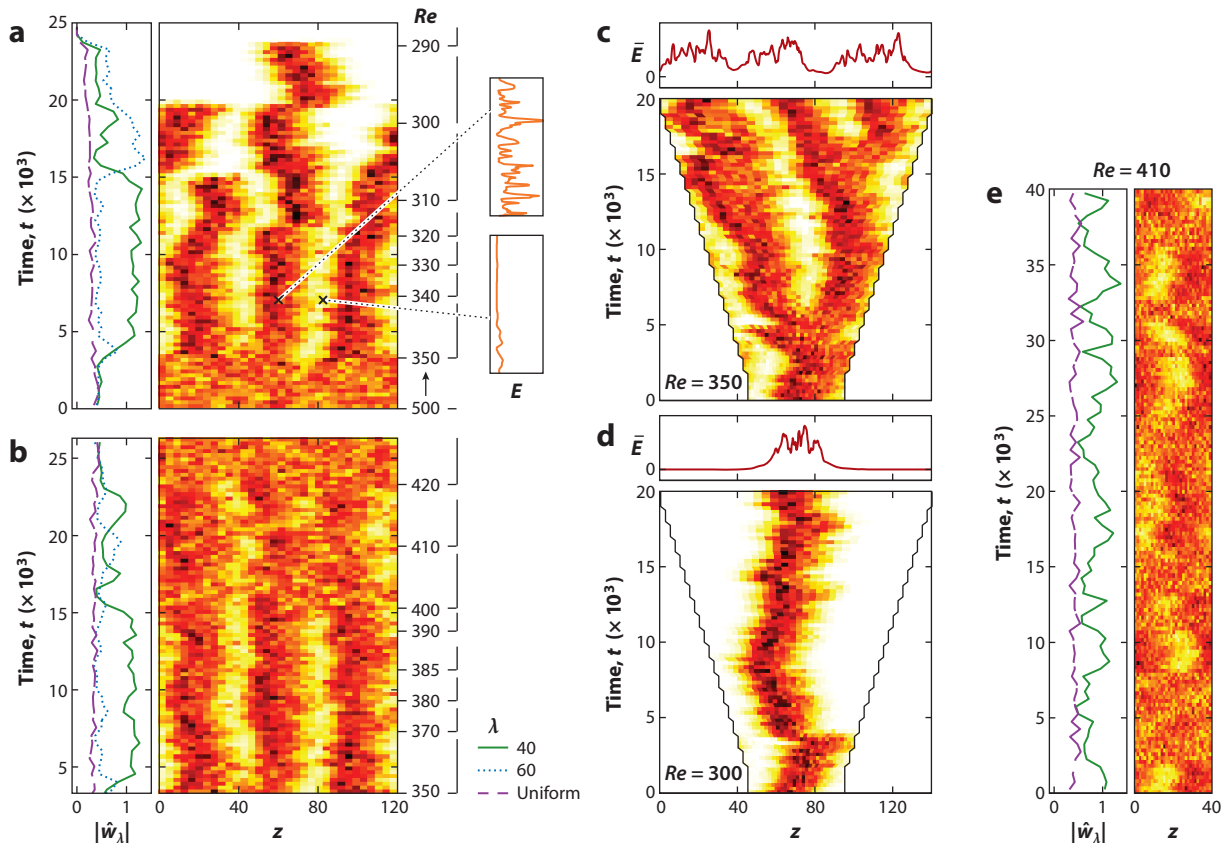


Figure 6

Different regimes of turbulent–laminar banded patterns in plane Couette flow. Spatiotemporal diagrams are constructed by sampling the kinetic energy at 32 points along a line at the mid-gap $y = 0$ in the long direction, z , averaging over temporal windows of length $T = 500$ and using colors varying from white (zero; laminar flow) to black (turbulent). For panels *a* and *b*, the domain length is $L_z = 120$. In panel *a*, we start with uniform turbulence and lower the Reynolds number from $Re = 500$. Three lighter laminar patches appear at $Re = 350$, leading to a wavelength of 40. Near $Re = 310$, one of the patches disappears, leading to a wavelength of 60, and near $Re = 300$, another disappears, leading to a single patch, which disappears at $Re = 290$. Plots to the right in panel *a* show detailed evolution of the kinetic energy within the temporal window in turbulent and laminar regions. In panel *b*, the initial condition is the turbulent–laminar banded pattern at $Re = 350$, which evolves to uniform turbulence when the Reynolds number increases. In panels *c* and *d*, the domain length increases in small discrete steps from $L_z = 50$ to $L_z = 140$. For $Re = 350$ (*c*), the turbulent region splits to retain an approximate wavelength of 40, while for $Re = 300$ (*d*), its width remains constant, corresponding to a single localized band. Plots above panels *c* and *d* of the final instantaneous turbulent kinetic energy show that for $Re = 350$, the turbulent kinetic energy remains above zero throughout the domain, whereas for $Re = 300$, it is zero in the laminar region. In panel *e*, with Re fixed at the intermediate value of 410 and L_z fixed at 40, the state remains poorly defined, with turbulent patches appearing and disappearing. Plots to the left of panels *a*, *b*, and *e* show the variation in time of the one-dimensional spatial Fourier components of the spanwise velocity, with the solid, dotted, and long-dashed curves corresponding to the $\lambda = 40$, $\lambda = 60$, and uniform components, respectively. All lengths are in units of the half-gap, b ; time, t , is in advective units, b/U , where U is the velocity of the walls.

Figure 6 illustrates various regimes of turbulent–laminar patterns as a function of Reynolds number. Spatiotemporal diagrams have been produced by sampling simulations in tilted domains along a line in the (long) band-perpendicular direction, z . The Reynolds number or the domain size is also changed over the course of some of the simulations. **Figure 6a** shows the evolution to the patterned state as the Reynolds number decreases. Time evolves upward and as it does

Re is decreased in steps, as shown at the right of the panel. At $Re = 500$ the flow is in a state of uniform, or featureless, turbulence. Following a decrease to $Re = 350$, a distinct pattern forms with three turbulent bands alternating with regions of quasi-laminar flow. As Re is further decreased, one turbulent band is lost at $Re = 310$ and a second is lost at $Re = 300$, leaving a single band that subsequently fully relaminarizes at $Re = 290$. The general trend shown in **Figure 6a** is robustly observed with decreasing Reynolds number, but the details vary with the realization. This Reynolds number scan is coarse; more precise thresholds and means of determining them are described below. In particular, patterned states that appear to be stable may ultimately revert to laminar flow on very long timescales. **Figure 6b** shows the reverse transition from a turbulent–laminar banded pattern to uniform turbulence as the Reynolds number is increased from 350 to 420. **Figure 6c** shows that if the Reynolds number is fixed at 350 and the domain size increases, a turbulent band repeatedly splits in order to retain a wavelength of about 40. The same procedure for $Re = 300$ in **Figure 6d** shows a single isolated band, independent of the domain size. This localized band is expected to revert to laminar flow on some very long timescale. In **Figure 6e**, Re is 410 and the domain size is fixed at 40. Laminar and turbulent patches repeatedly appear and disappear. In all of the cases shown in **Figure 6**, when laminar patches appear, the intensity of the turbulence within the bands increases, keeping the total turbulent intensity approximately constant.

A quantitative characterization of the pattern is provided by the line graphs to the left of panels *a*, *b*, and *e* in **Figure 6**. These show the time-dependent moduli $|w_\lambda|$ of the coefficients of the one-dimensional spatial Fourier transform (in the band-perpendicular direction) of the spanwise velocity at mid-gap averaged over intervals of $\Delta T = 500$. These provide a good characterization of the patterns, with significant $\lambda = 40$ and $\lambda = 60$ components at appropriate times, and it is this information that has been used to determine a threshold. **Figure 7a** presents the Reynolds number dependence of the spectral coefficient $\langle |\hat{w}_{\lambda=40}| \rangle$, where averages have been taken over long time series, such as **Figure 6e**. A clear transition is seen near $Re = 430$, which we take to be the threshold between uniform turbulence and turbulent–laminar bands in plane Couette

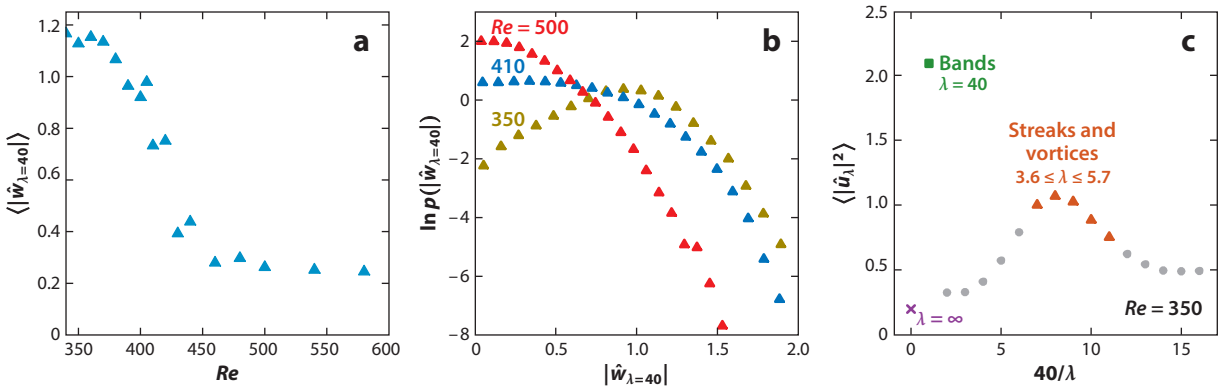


Figure 7

Modulus $|\hat{w}_{\lambda=40}|$ of the $\lambda = 40$ Fourier component in the band-perpendicular direction of the spanwise velocity at mid-gap, such as shown in **Figure 6e**. (a) Average over time series. A transition between uniform turbulence and a pattern is seen near Reynolds number (Re) 430. (b) Logarithm of the probability distribution function for a uniformly turbulent flow at $Re = 500$, an intermittent flow at $Re = 410$, and a turbulent–laminar pattern flow at $Re = 350$. The most probable value is zero for uniform turbulence but has a finite value for a patterned flow. (c) Time-averaged band-perpendicular square Fourier component of the streamwise velocity, $|\hat{u}_\lambda|^2$, at $Re = 350$. The dominant coefficient corresponding to bands has a wavelength of $\lambda = 40$, while coefficients corresponding to streamwise vortices and streaks have $3.6 \leq \lambda \leq 5.7$. Figure adapted with permission from Tuckerman & Barkley (2011).

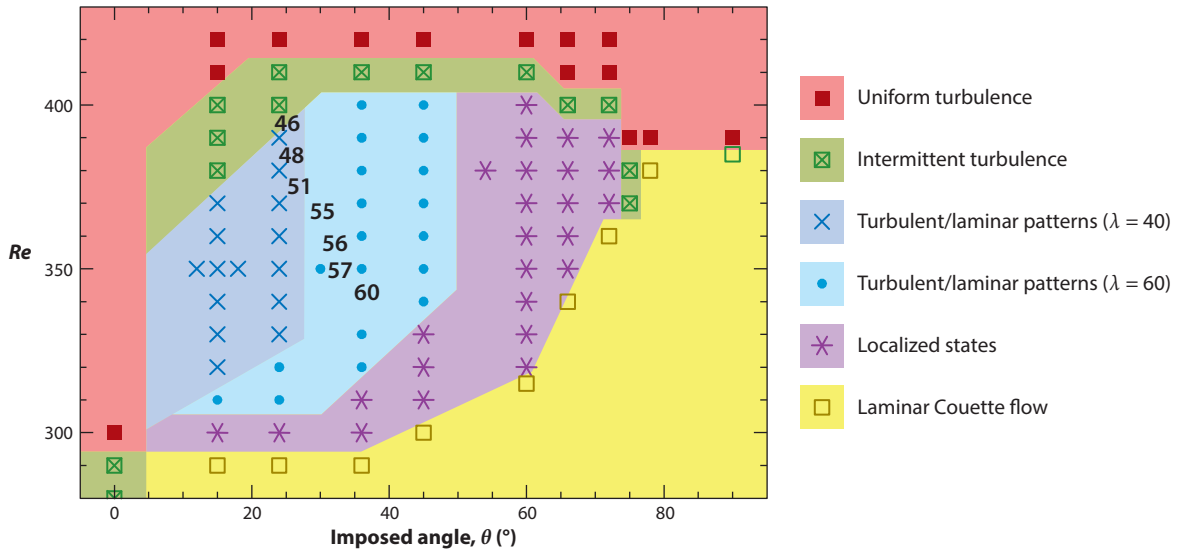


Figure 8

Survey of turbulent–laminar patterned regimes in our computations of plane Couette flow in a narrow tilted rectangular domain as a function of imposed angle θ and Reynolds number Re . Black numbers show wavelengths (in units of the half-gap, b) found in experiments of Prigent et al. (2003) at indicated values of θ and Re . Figure adapted with permission from Tuckerman & Barkley (2011).

flow in our narrow tilted rectangular domain. (Much of Section 5 is devoted to characterizing the lower threshold that separates laminar flow from the presence of turbulence.) **Figure 7b** constructs probability distribution functions from these long time series by averaging over intervals of $\Delta T = 500$. At $Re = 500$, when the turbulence is uniform, the most probable value of $|\hat{w}_{\lambda=40}|$ is 0. At $Re = 410$, the distribution undergoes an inflection and by $Re = 350$, when a turbulent–laminar pattern with $\lambda = 40$ is robust, the most probable value is nonzero. Finally, **Figure 7c** presents the entire Fourier spectrum at $Re = 350$, contrasting the coefficients corresponding to the bands, with $\lambda = 40$, with those of the much smaller structures, with $\lambda \approx 4$, twice the gap of size 2. These smaller structures, as seen in **Figure 2a**, consist of streamwise vortices (wall-normal and spanwise flow) and streaks (spanwise dependence of the streamwise velocity). At mid-gap, their mean spanwise velocity is zero and hence we show the streamwise components, $|\hat{u}_\lambda|$.

Finally, **Figure 8** presents a survey of the regimes that are seen in MBUs as a function of imposed angle θ and Reynolds number. The experiments of Prigent et al. (2003) show wavelengths (in the band-perpendicular direction) that increase from 46 to 60 half-gaps and angles that increase from 25° to 37° as the Reynolds number decreases, as can also be seen in **Figure 3b,c**. Because the angle is imposed in tilted MBU domains, simulations can compute patterns with a much wider range of both angles and wavelengths. Most of these are presumably unstable when placed in a larger, less constrained domain since they have not been observed. For $15^\circ \leq \theta \leq 72^\circ$, we use a tilted domain whose dimensions are $[4/\sin \theta, 2, 120]$ and find periodic or localized bands. Simulations in a nontilted domain with a long streamwise length of 220 and a short spanwise direction of length 4 (corresponding to 90°) show direct laminarization at $Re \approx 400$ after a very short-lived transient pattern. In contrast, simulations with a long spanwise length of 120 and a short streamwise length of 10 (corresponding to 0°) show repeated nucleation of turbulent regions, which persists to Reynolds numbers as low as $Re \approx 200$ (see Barkley & Tuckerman 2005b).

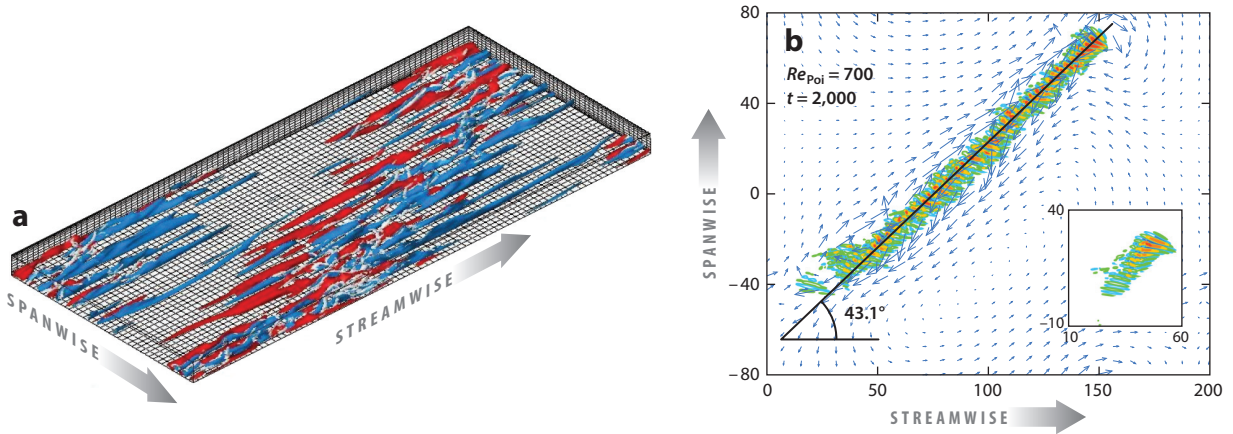


Figure 9

Turbulent bands in plane Poiseuille flow. (a) Three-dimensional view of the deviation from laminar flow of streamwise velocity at Reynolds number (Re_{Poi}) 1,140 in the lower half of a $[51.2, 2, 22.5]$ domain from Tsukahara et al. (2006). (b) Wall-normal velocity (colors) and horizontal mean flow (arrows) at $Re_{\text{Poi}} = 700$ in a $[200, 2, 160]$ domain from Xiong et al. (2015). The inset is the initial condition. All lengths are in units of the half-gap, b ; time, t , is in advective units, b/U , where U is $3/2$ of the bulk velocity. Panels adapted with permission from (a) Tsukahara et al. (2006) and (b) Xiong et al. (2015).

3. POISEUILLE FLOW: TWO SUPERPOSED SHEAR LAYERS

Turbulent–laminar banded patterns also exist in plane Poiseuille flow, sometimes called channel flow, the flow between two parallel rigid plates maintained at a constant distance and driven by an imposed streamwise pressure gradient or flux (see **Figure 9**). Banded patterns were observed first numerically in plane Poiseuille flow by Tsukahara et al. (2005, 2006) and experimentally by Hashimoto et al. (2009), with later simulations by Brethouwer et al. (2012), Fukudome & Iida (2012), Tuckerman et al. (2014), Xiong et al. (2015), Kushwaha et al. (2017), and Tao et al. (2018).

The properties of transitional plane Poiseuille flow resemble those of plane Couette flow. However, the similarities are somewhat masked by the trivial fact that the two flows effectively use different nondimensionalization. Plane Poiseuille flow can be viewed as the superposition of two shear layers of opposite sign. Thus, the characteristic length scale in plane Poiseuille flow—the half-channel height—is the full height of one of these shear layers. In contrast, the half-channel height in the Couette flow convention is half its shear layer height. In addition, several different conventions are used for the velocity scale in plane Poiseuille flow. Here we consider the system driven by an imposed flux, rather than imposed pressure gradient. Hence, the mean streamwise velocity U_{bulk} is known. We use as a velocity scale $U \equiv 3U_{\text{bulk}}/2$, which is the centerline velocity of laminar flow with mean velocity U_{bulk} . The velocity scale, U , is then the difference between the maximum and minimum velocity of laminar Poiseuille flow. However, in Couette flow, the velocity scale used is half the difference of the velocities of the two walls. As a result, in terms of the shear, both the length scale and the velocity scales used for nondimensionalization in plane Poiseuille flow are twice those used in plane Couette flow. Thus, roughly speaking, one should expect values of Re_{Poi} , as conventionally defined, to differ from values of Re_{Cou} by a factor of four,

$$\mathbf{u}_{\text{Poi}}^{\text{lam}} = U \left(1 - \frac{y^2}{b^2} \right) \mathbf{e}_{\text{strm}}, \quad Re_{\text{Poi}} \equiv \frac{U b}{\nu} = \frac{4 \left(\frac{U}{2} \right) \left(\frac{b}{2} \right)}{\nu} \approx 4 Re_{\text{Cou}}, \quad 3.$$

where Re_{Cou} uses plane Couette conventions based on each single-sign shear layer.

Plane Poiseuille flow also differs from plane Couette flow in its symmetries. Plane Couette flow possesses centro-symmetry, i.e., simultaneous reflection in the streamwise and wall-normal directions. In contrast, although plane Poiseuille flow has reflection symmetry in the wall-normal direction, it is not symmetric between the upstream and downstream directions. Therefore turbulent–laminar bands in plane Couette flow are stationary, at least on short timescales, while in plane Poiseuille flow, they generically travel in the streamwise direction since there is no symmetry to keep them stationary.

Figure 10 shows results from simulations for plane Poiseuille flow in a tilted MBU domain with dimensions [10, 2, 40]. The simulations use the pseudospectral Chebyshev/Fourier `ChannelFlow 2.0` code (J.F. Gibson, F. Reetz, S. Azimi, A. Ferraro, T. Kreilos, et al., manuscript in preparation) with 12 points per unit horizontal length and 32 per unit wall-normal length. The protocol is similar to that used in the previous plane Couette simulations: The Reynolds number is decreased in discrete steps during the simulation. Results are shown in a frame of reference moving at the mean velocity, U . **Figure 10a** shows that, starting from uniform turbulence and decreasing the Reynolds number, the approximate threshold for the appearance of the bands is $Re_{\text{Poi}} \approx 1,900 = 475 \times 4$; that for localized bands, the threshold is $Re_{\text{Poi}} \approx 1,300 = 325 \times 4$; and that for relaminarization, the threshold is $Re_{\text{Poi}} \approx 800 = 4 \times 200$ in the MBU. Rather than a typical wavelength of 40 half-gaps, the wavelength at onset is 20 half-gaps, i.e., 40 quarter-gaps, the natural comparison to use with plane Couette flow. The traveling character of the turbulent–laminar patterns is evident. Patterns travel more quickly than the mean flow for $Re_{\text{Poi}} \lesssim 1,100$ and more slowly for $Re_{\text{Poi}} \gtrsim 1,100$; the velocities range from approximately $0.03 U$ to $-0.03 U$. **Figure 10b–d** also shows cross sections of time and band direction–averaged fields (see also Tsukahara et al. 2006). The streamwise velocity alternates between a parabolic and flattened profile, the streamfunction shows two superposed elongated recirculation cells, and the turbulent kinetic energy is concentrated near the two bounding walls.

We now consider the various forces that must be in equilibrium to maintain a statistically permanent turbulent–laminar banded pattern and that dominate in the turbulent or laminar regions. We write the averaged Navier–Stokes equation,

$$0 \approx \underbrace{-\langle(\tilde{\mathbf{u}} \cdot \nabla)\tilde{\mathbf{u}}\rangle}_{F_{\text{turb}}} + \underbrace{-\langle\mathbf{u}^{\text{lam}} \cdot \nabla(\mathbf{u} - \mathbf{u}^{\text{lam}})\rangle}_{F_{\text{adv}}} + \underbrace{\frac{1}{Re}\nabla^2\langle\mathbf{u} - \mathbf{u}^{\text{lam}}\rangle}_{F_{\text{visc}}}. \quad 4.$$

Equation 4 omits the largest forces, which balance to maintain the laminar flow, as well as some of the negligibly smallest forces. We have projected onto the streamwise direction to define F_{turb} , the turbulent or Reynolds stress force; F_{adv} , expressing the dominant advection by the laminar flow; and F_{visc} , the viscous force countering curvature. **Figure 10** shows these forces at three wall-normal locations as a function of z for a turbulent band for both Poiseuille and Couette flow. The relation between the forces above and below mid-gap respect the symmetries of the Poiseuille and Couette configurations, while the relation between the forces in the Poiseuille and Couette flows confirms the interpretation of Poiseuille flow as two superposed Couette flows. Recalling that z has a component in the streamwise direction and given the signs of Poiseuille and Couette flow in the upper and lower halves of the channel, F_{turb} mostly acts to accelerate the fluid in the streamwise direction and F_{visc} acts to oppose it. The term F_{adv} changes sign as the band is traversed. The Couette turbulent band is localized: In the laminar region with $F_{\text{turb}} = 0$, we also have $F_{\text{adv}} = F_{\text{visc}} = 0$. The Poiseuille turbulent band, however, is bordered by regions for which $F_{\text{turb}} = 0$ but F_{adv} and F_{visc} are equal and opposite, though small.

An interesting feature of plane Poiseuille flow is that a localized perturbation may evolve into isolated oblique turbulent bands by extending from only one of its endpoints, as in **Figure 9b**,

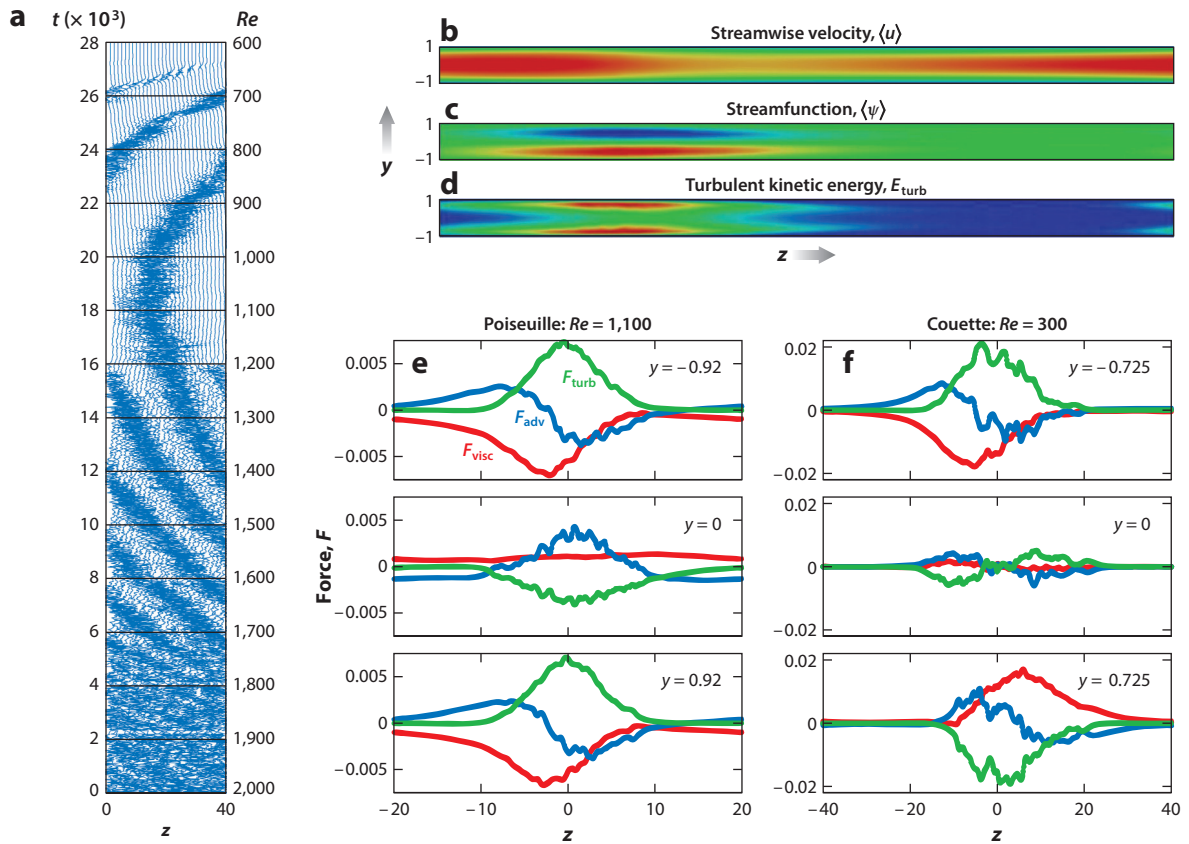


Figure 10

(a) Evolution of a simulation of plane Poiseuille flow in a long narrow tilted rectangular channel in the frame of the streamwise bulk velocity. The simulation is initialized with uniform turbulence at Reynolds number (Re_{Poi}) 2,000, which is decreased in steps of 100. Plotted are spanwise velocity time series at 32 points along a line at $y = 0.8$. Laminar bands with wavelength 20 emerge at around $Re_{\text{Poi}} \approx 1,900$, with the wavelength increasing to 40 at $Re_{\text{Poi}} \approx 1,200$ and turbulence disappearing at $Re_{\text{Poi}} \approx 800$. The pattern moves more slowly than the bulk velocity for $Re_{\text{Poi}} \gtrsim 1,100$ and more quickly for $Re_{\text{Poi}} \lesssim 1,100$. (b–d) Temporally and band-averaged fields for $Re = 1,100$. (b) The streamwise velocity $\langle u \rangle$ (including laminar profile) alternates between a parabolic profile in y , in which the maximum value of $\langle u \rangle$ is high, and a flattened profile, in which it is low. (c) The streamfunction $\langle \psi \rangle$ in the (y, z) plane shows two superposed elongated recirculating cells. (d) Turbulent kinetic energy E_{turb} shows that the turbulence is localized near the walls, where the shear is highest. (e, f) The streamwise Reynolds stress (green), advective (blue), and viscous (red) forces as a function of z at three y locations for the mean flow associated with turbulent–laminar band in Poiseuille flow (e) at $Re_{\text{Poi}} = 1,100$ and in Couette flow (f) at $Re_{\text{Cou}} = 300$. For both flows, F_{turb} acts in the same direction as the laminar profile, while F_{visc} is in the opposite direction. The balance of forces is very similar for the $y > 0$ and $y < 0$ sections of Poiseuille flow and the $y < 0$ section of Couette flow. The force balance for the $y > 0$ section of Couette flow is related by centro-symmetry to the force balance for the $y < 0$ section of Couette flow. All lengths are in units of the half-gap, b ; time, t , is in advective units, b/U , where U is $3/2$ of the bulk velocity. Figure adapted with permission from Tuckerman et al. (2014).

adapted from Xiong et al. (2015). This is another manifestation of the asymmetry between the upstream and downstream streamwise directions of plane Poiseuille flow: Unlike in plane Couette flow, here the two ends of a single band experience a different relationship to the streamwise flow. Spreading is observed to start at $Re_{\text{Poi}} = 660$. Above this Reynolds number, localized turbulent bands increase steadily in length in sufficiently large domains or sustain themselves in a cycle of band extension and breakup in periodic domains (Xiong et al. 2015, Kanazawa 2018, Tao et al. 2018).

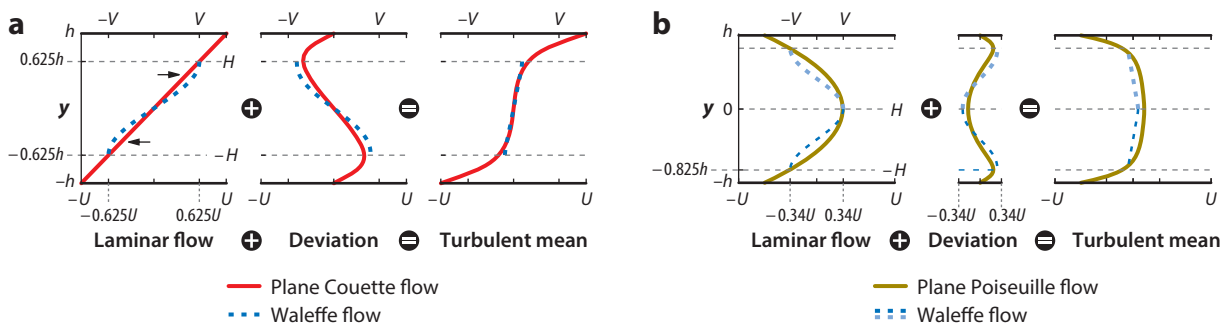


Figure 11

Correspondence between flows with rigid and with free-slip walls. (a) Plane Couette flow and Waleffe flow. The wall-normal bounds $\pm H$ of the Waleffe flow domain and its velocity extrema $\pm V$ are matched to those of the interior portion of the turbulent mean profile of plane Couette flow with wall-normal bounds $\pm b$ and velocity extrema $\pm U$. (b) Plane Poiseuille flow and its free-slip version as two superposed Waleffe flows, each occupying a height $2H$. Figure adapted with permission from Chantry et al. (2016).

4. WALEFFE FLOW: ROLE OF THE WALLS

An important question is the role of walls in wall-bounded shear flows, assumed in their very name. The necessity for rigid walls was questioned by Waleffe (1997), who derived his classic self-sustaining process not from wall-bounded plane Couette flow, but from a simplified version in which the no-slip boundary conditions $u = v = w = 0$ at $y = \pm 1$ are replaced by free-slip conditions $\partial_y u = v = \partial_y w = 0$. The flow is still confined between boundaries; however, it is not driven by wall motion or by a pressure gradient, but instead by an imposed bulk force varying sinusoidally in the wall-normal direction, y .

Figure 11a shows the correspondence between plane Couette flow and Waleffe flow. In plane Couette flow, the laminar profile is straight, while the mean turbulent profile takes a sigmoidal form with sharp changes near the boundaries and is nearly linear in the interior, corresponding to constant mean shear. In contrast, in Waleffe flow, the laminar profile is sinusoidal while the mean turbulent profile is roughly linear, corresponding to a constant shear. If the domain of Waleffe flow is taken to be the interior of plane Couette flow, as in Figure 11a, then Waleffe flow can be viewed as modeling only this region, without the near-wall regions (Chantry et al. 2016).

Figure 11a indicates a specific scaling based on this correspondence: The height H of the Waleffe domain is 0.625 times the height b of the plane Couette domain, and the maximum speed V of the Waleffe profile is correspondingly 0.625 times the speed U of the plane Couette profile. This height, that of the inner near-linear portion of the mean turbulent plane Couette flow profile, is not universal but varies slowly with Re in the transition region. We define a Reynolds number Re for Waleffe flow, based on the correspondence with plane Couette flow, i.e.,

$$\mathbf{u}_{\text{Wal}}^{\text{lam}} = V \sin\left(\frac{\pi y}{2H}\right) \mathbf{e}_{\text{strm}}, \quad Re \equiv \frac{Ub}{\nu} = \frac{V/0.625 \times H/0.625}{\nu}, \quad 5.$$

where the notation is defined in Figure 11. Simulations are carried out by adapting Channelflow 2.0 (J.F. Gibson, F. Reetz, S. Azimi, A. Ferraro, T. Kreilos, et al., manuscript in preparation) for the free-slip conditions, on a grid with 12 points per horizontal unit length and 15 per wall-normal unit length.

Waleffe flow undergoes the same sequence of transitions as plane Couette flow as the Reynolds number is decreased, from uniform turbulence through regular turbulent–laminar bands, then isolated and fragmented bands, and finally to laminar flow. Turbulent–laminar patterns exist in

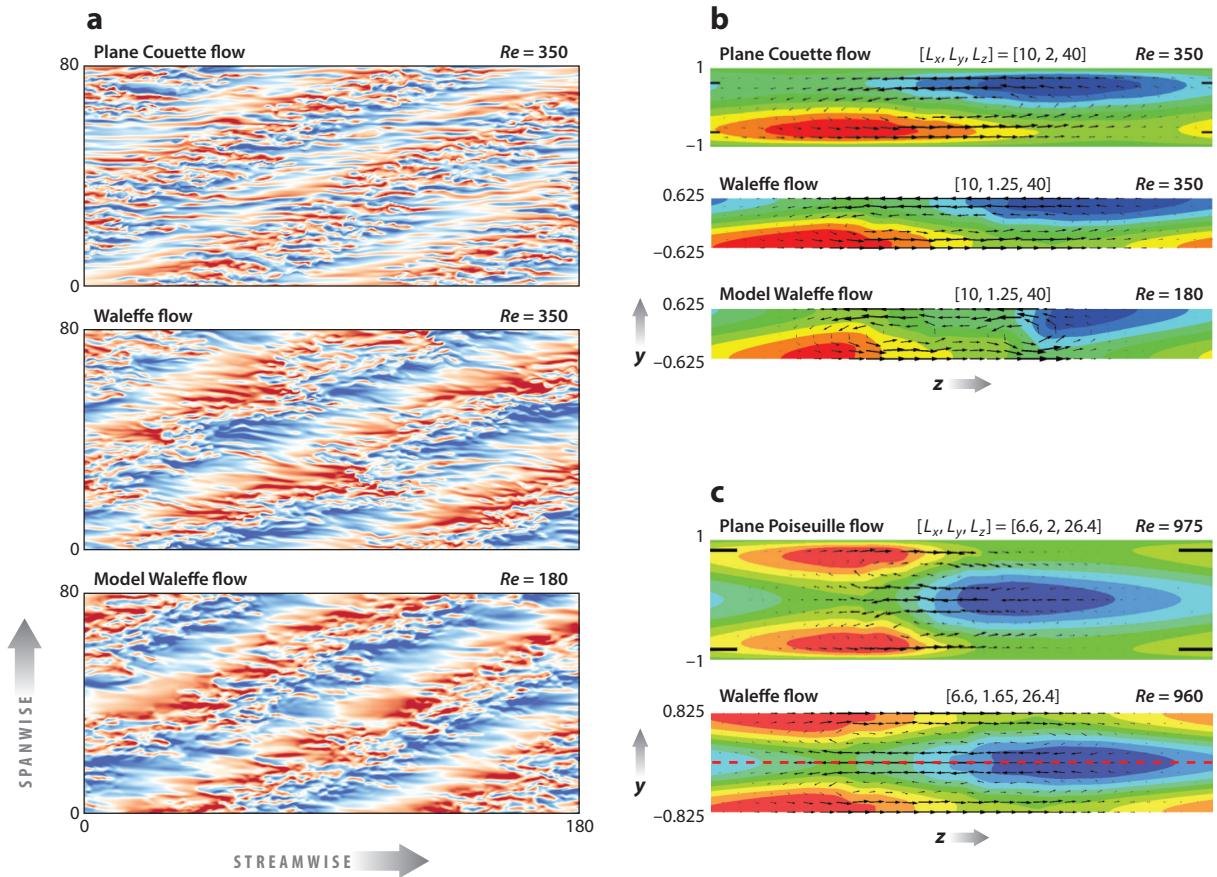


Figure 12

(a) Banded turbulence visualized by instantaneous streamwise velocity at the midplane, with contours from negative (blue) to positive (red) velocity in plane Couette flow (PCF), Waleffe flow (WF), and model Waleffe flow (MWF). (b) Mean flow for turbulent laminar patterns in PCF, WF, and MWF and (c) their plane Poiseuille equivalents, PPF and WF. Flows are calculated in a tilted domain like that of **Figure 2b**, and averages are taken in time and in the band-parallel direction. Planes shown are in the band-perpendicular direction, z , and in the wall-normal direction, y . Arrows show the flow in these planes, while colors show the magnitude of the flow in the band-parallel direction. The y -direction has been stretched by a factor of 3, and black horizontal tick marks in (b) PCF and (c) PPF indicate the bounds of the interior region to which WF corresponds. Lengths are in units of the half-gap, b , for PCF and PPF. For WF and MWF, b is the half-gap of the corresponding wall-bounded PCF and PPF flows. Figure adapted with permission from Chantry et al. (2016).

Waleffe flow approximately for $Re \in [250, 640]$, a wide range that encompasses the corresponding range for plane Couette flow. **Figure 12** compares the patterns for both flows. Horizontal views of the instantaneous flows, as well as vertical views of the averaged flows computed in the MBU, show the marked resemblance between the patterns. Model Waleffe flow (MWF), also shown in this figure, is discussed below.

The free-slip version of plane Poiseuille flow is constructed explicitly as a superposition of two free-slip Couette flows, or equivalently, as a free-slip channel driven by a body force with y dependence, $\cos(\pi y/H)$, as shown in **Figure 11b**. There are two provisos. First, rigid-wall plane Poiseuille flow has two boundary layers that are to be clipped, rather than the four that would exist in two superposed rigid-wall plane Couette flows, leading to slightly different scalings. (Compare

the domain sizes in **Figure 12c** with those in **Figure 12b**.) Second, a Tollmien–Schlichting-like eigenmode that would otherwise be unstable at transitional Reynolds numbers must be suppressed. The appropriate scaling and Reynolds number definition, turbulent–laminar bands are then present in free-slip plane Poiseuille flow for Re_{Poi} between 700 and 1,800, close to the range found for the rigid case (see **Figure 10a**). The temporally and spatially band-parallel averaged flows in **Figure 12** highlight the resemblance between these flows in the rigid-wall and free-slip versions, as well as the interpretation of plane Poiseuille flow as two superposed plane Couette flows (see also **Figures 5** and **10**, in which the wall-normal direction is not stretched).

Other ideas for simulating fully turbulent channel flow at higher Reynolds numbers in the interior region only have been proposed by Podvin & Fraigneau (2011) and Mizuno & Jiménez (2013), who substituted for the no-slip boundary condition at the wall a synthetic velocity field imposed at an interior, off-wall boundary.

5. MODEL WALEFFE FLOW: DIRECTED PERCOLATION

We have seen that rigid walls are not necessary to reproduce the basic phenomenology of transition to turbulence in plane Couette and Poiseuille flows. This fact has not only important theoretical consequences, but also practical ones, since this allows the high wall-normal resolution requirements of boundary layers to be avoided. We take a step further and seek a minimal model in the wall-normal direction that reproduces the phenomenology of transitional plane Couette flow. We expand (u, v, w) in low-order trigonometric functions as follows,

$$\begin{aligned} u(x, y, z) &= u_0(x, z) + u_1(x, z) \sin(\beta y) + u_2(x, z) \cos(2\beta y) + u_3(x, z) \sin(3\beta y), \\ v(x, y, z) &= v_1(x, z) \cos(\beta y) + v_2(x, z) \sin(2\beta y) + v_3(x, z) \cos(3\beta y), \\ w(x, y, z) &= w_0(x, z) + w_1(x, z) \sin(\beta y) + w_2(x, z) \cos(2\beta y) + w_3(x, z) \sin(3\beta y), \end{aligned} \quad 6.$$

with $\beta = \pi/(2H)$. To ensure incompressibility, we use a poloidal–toroidal plus mean-mode representation,

$$\mathbf{u} = f(y)\mathbf{e}_x + g(y)\mathbf{e}_z + \nabla \times \psi(x, y, z)\mathbf{e}_y + \nabla \times \nabla \times \phi(x, y, z)\mathbf{e}_y, \quad 7.$$

where f , g , and ψ match the y -formulation of u , and ϕ matches that of v . Because ψ and ϕ are taken to be periodic in x and z , their derivatives cannot produce functions that are constant in x and z , and so the mean modes f and g must be included explicitly to achieve a general, valid representation of \mathbf{u} (e.g., Marqués 1990). Substituting Equation 7 into the Navier–Stokes equations and applying Fourier orthogonality in y , we derive our governing equations, which are seven partial differential equations in (x, z, t) and six ordinary differential equations (ODEs) for the non-constant components of f and g . The original eight-ODE model, derived by Waleffe (1997) to illustrate the self-sustaining process, is contained within the system and can be recovered by reducing the number of modes in y and imposing a single Fourier wave number in x and z . Our model is inspired by a series of models (Manneville & Locher 2000, Moehlis et al. 2004, Lagha & Manneville 2007, Seshasayanan & Manneville 2015) of plane Couette and Waleffe flow.

Not only can the degrees of freedom economized in the wall-normal direction be used to increase the horizontal degrees of freedom, but since the length scales in the horizontal directions tend to mimic those in the wall-normal direction, the elimination of the boundary layers leads to economy of resolution in the horizontal directions as well. In particular, only four modes per horizontal spatial unit are needed, compared with ten for plane Couette flow.

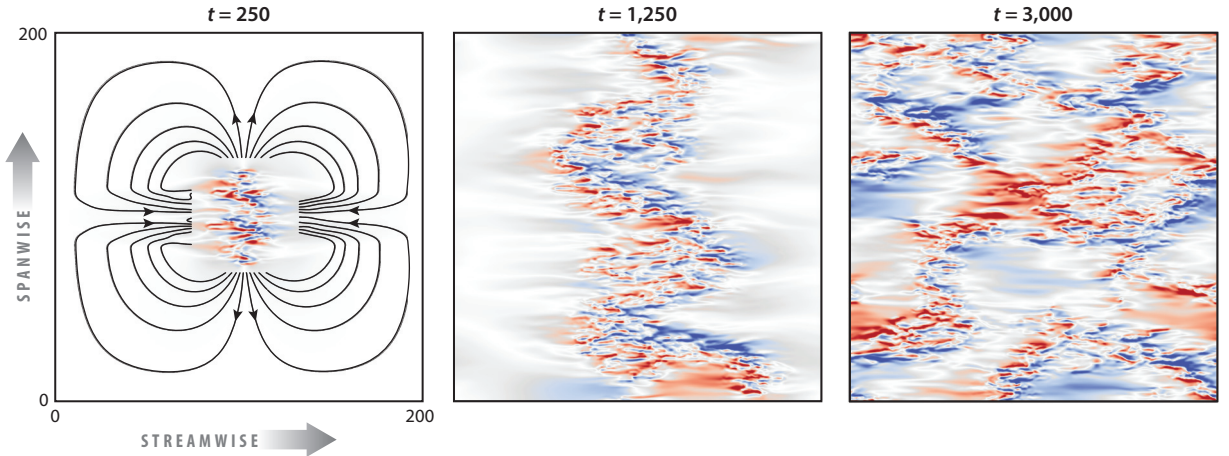


Figure 13

Growth of a turbulent spot in model Waleffe flow. The flow is initialized with a poloidal vortex, and the subsequent evolution is visualized by streamwise velocity at the midplane. At early times ($t = 250$), a large-scale quadrupolar flow dominates, as shown by streamlines of the y -averaged flow (*contour lines*, only plotted away from the spot for visibility). By $t = 1,250$, bands begin to develop and form a zigzag across the domain. The bands continue to grow, and by $t = 3,000$, a complex array of bands fills the domain. All lengths are in units of b ; time, t , is in advective units, b/U , where b and U are respectively the half-gap and velocity of the corresponding plane Couette flow, as in **Figure 11**. Figure adapted with permission from Chantry et al. (2016).

In simulations performed in very large domains, a horizontal drag force, sometimes called Rayleigh or Ekman friction,

$$\mathbf{F}_{\text{Rayl}} \equiv -\sigma(w\mathbf{e}_x + w\mathbf{e}_z), \quad 8.$$

is added to the Navier–Stokes equations. This force damps all modes, but its effect is only significant on modes with no vertical curvature and little horizontal curvature. These modes would otherwise decay extremely slowly in Waleffe flow and are absent in Couette flow. The value $\sigma = 10^{-2}$ reproduces the damping to which these modes would be subjected in the wall regions of the corresponding Couette flow.

MWF displays qualitatively the same transitional phenomena as Waleffe flow and plane Couette flow, but at lower Reynolds numbers. The turbulent–laminar bands shown for MWF in **Figure 12a,b** occur in the approximate Reynolds number range of $[125, 230]$, using the definitions given in Equation 5. Inclusion of the drag force of Equation 8 shifts upward the Reynolds number necessary to produce the same phenomena, but these values still remain far below those for plane Couette or Waleffe flow.

Figure 13 shows a simulation at $Re = 160$ starting from an initial vortex, following Schumacher & Eckhardt (2001). A localized turbulent spot develops, with its corresponding large-scale quadrupolar flow, followed by a spanwise elongated turbulent patch and finally a complex banded form. This evolution matches that seen in simulations of plane Couette flow by Duguet et al. (2010) and Duguet & Schlatter (2013). The turbulent spot in the early stage of development was first studied in plane Couette flow by Lundbladh & Johansson (1991) and Tillmark & Alfredsson (1992). More recently, the evolution of spots has been investigated as a means to understand the mechanisms of turbulent–laminar interface growth, as well as the development and role of large-scale flows (see Duguet & Schlatter 2013; Lemoult et al. 2014; Couliou & Monchaux 2015, 2018).

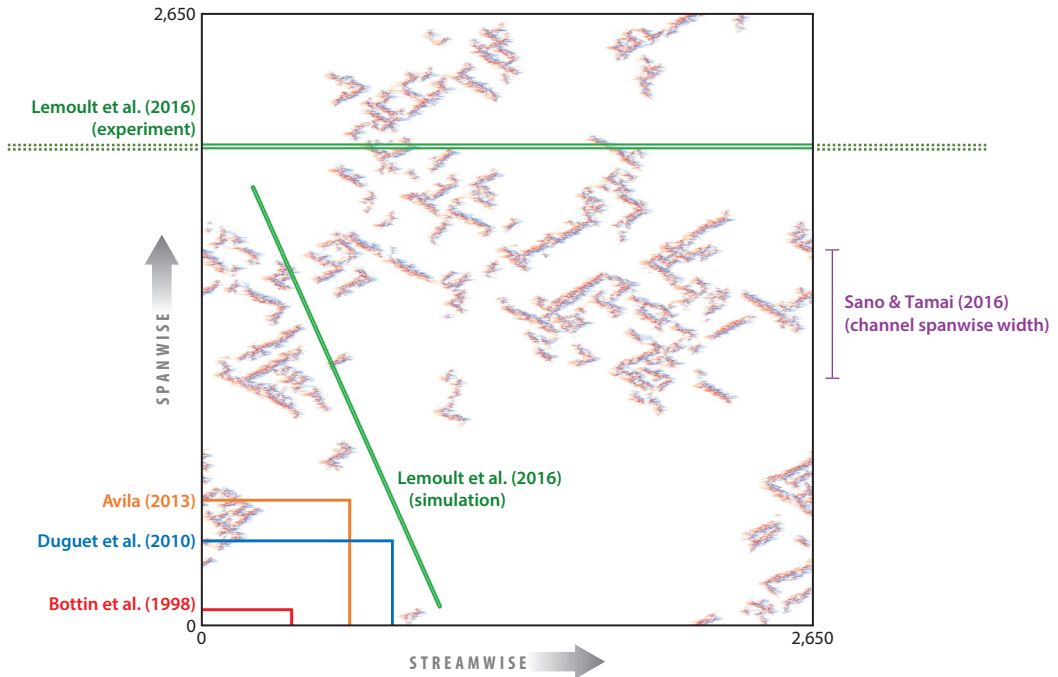


Figure 14

Instantaneous depiction of intermittent turbulence just above the onset of sustained turbulence. The streamwise velocity in the midplane is shown for a simulation of model Waleffe flow in a domain with dimensions $[2,560, 1.25, 2,560]$ at $Re = 173.824$ (reduced Reynolds number $\epsilon = 1.4 \times 10^{-4}$) with Rayleigh friction factor $\sigma = 10^{-2}$ after 1.2×10^6 time units. Laminar flow is seen as white. The turbulence fraction is $F_t \approx 0.1$. Experimental and numerical domains of Bottin et al. (1998), Duguet et al. (2010), and Avila (2013) and are overlaid in red, blue, and orange, respectively. Part of the quasi-one-dimensional domain of Lemoult et al. (2016) is shown in green, and the spanwise width of the plane Poiseuille experiment of Sano & Tamai (2016) is indicated in purple on the right. All lengths are in units of b ; time, t , is in advective units, b/U , where b and U are respectively the half-gap and velocity of the corresponding plane Couette flow. Figure adapted with permission from Chantry et al. (2017).

In the previous sections, we have mentioned lower bounds for the existence of isolated bands, but these have been only approximate. A long-standing and fundamental question has been whether the transition to turbulence is discontinuous or continuous. The CEA-Saclay group (Daviaud et al. 1992, Bottin & Chaté 1998, Bottin et al. 1998) has extensively investigated this question for plane Couette flow; Manneville & Dauchot (2001) and Manneville (2015) have stressed that the question must be addressed in the spatiotemporal context.

We have used MWF to answer this question (Chantry et al. 2017) by carrying out simulations in an extremely large domain of size $[2,560, 1.25, 2,560]$. **Figure 14** shows the instantaneous streamwise velocity at the midplane for such a simulation, at $Re = 173.824$ with $\sigma = 10^{-2}$, and illustrates precisely why such large domains are necessary for this type of study. The smaller domains used in past experiments and simulations, also shown in **Figure 14**, would be likely to detect no turbulence under these conditions, and this is in fact the case. We define the turbulent fraction F_t to be the fractional area of the horizontal domain for which the height-integrated energy of the deviation from laminar flow is greater than a threshold value, 0.01, i.e., the colored areas of **Figure 14**. For the large domain of **Figure 14**, a continuous dependence of F_t on Re is obtained, with a threshold of $Re_c \approx 173.80$, as shown in **Figure 15a**. For simulations of MWF carried out in a smaller domain of size $[380, 1.25, 70]$, **Figure 15b** shows that F_t behaves discontinuously with Re .

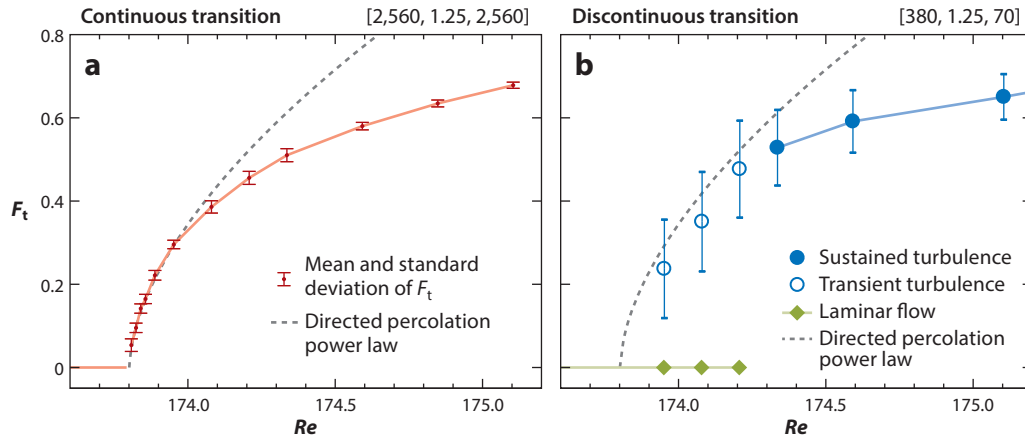


Figure 15

Bifurcation diagrams for the transition to turbulence. (a) Continuous transition in domain of size $[2,560, 1.25, 2,560]$. Equilibrium turbulence fraction (F_t) is plotted as a function of Reynolds number (Re). (b) Discontinuous transition in a domain of size $[380, 1.25, 70]$, approximately that of the experiments by Bottin & Chaté (1998). Figure adapted with permission from Chantry et al. (2017).

Philip & Manneville (2011) computed a discontinuous transition to turbulence in plane Couette flow whose Reynolds number threshold decreased with increasing domain size, but all of their domains were considerably smaller than any of those depicted in **Figure 14**. The transition to turbulence in MWF is continuous, but only in the limit of infinite domain size; even in **Figure 15a**, there exists a minimum nonzero value of F_t based on the domain size. In the classic hydrodynamic pattern-forming systems such as corotating Taylor–Couette flow or Rayleigh–Bénard convection, the transition is to a new state that exists everywhere but has infinitesimally small amplitude. In contrast, in MWF (and presumably also in plane Couette flow and Poiseuille flow), transition to turbulence occurs via the increasing density occupied by the turbulent state in an otherwise laminar background, not via its increasing amplitude in any given area or volume.

Our simulations of MWF demonstrate a more specific aspect of turbulent transition. Noting that in subcritical shear flows, turbulence can spread into laminar regions but cannot arise spontaneously, Pomeau (1986) postulated that this transition might belong to the universality class of directed percolation, an idea supported by Manneville & Dauchot (2001). This would imply not only that F_t varies continuously with Reynolds number, but also that power laws with specific predicted exponents would hold near onset. **Figure 15a** shows $F_t \sim \epsilon^\beta$, where ϵ is defined to be $(Re - Re_c)/Re_c$ and β has the value 0.583 predicted for directed percolation with two extended directions (Lübeck 2004). **Figure 16** shows the temporal evolution of F_t for various Reynolds numbers near Re_c . Above Re_c , F_t eventually saturates at the finite values plotted in **Figure 15a**, while below Re_c , F_t eventually decreases to zero. **Supplemental Video 2** shows the evolution of MWF in our large domain, for cases with $Re \approx Re_c$ and $Re > Re_c$. The theory of directed percolation makes quantitative predictions about this behavior (Lübeck 2004). When time and the turbulent fraction are rescaled to $t|\epsilon|^\nu$ and $t^\alpha F_t$, as shown in **Figure 16b**, where the exponents have the theoretical values of $\alpha \simeq 0.4505$ and $\nu \simeq 1.295$, the data collapse on two curves, one for above-critical evolution and the other for below-critical evolution.

Counter-rotating Taylor–Couette flow with a very narrow gap, and hence minimal curvature, has been used as a way of approaching plane Couette flow. Shi et al. (2013) carried out simulations of Taylor–Couette flow in a long tilted domain (MBU) like that of **Figure 2** in order to determine the typical statistical lifetimes as a function of Reynolds number for decay and splitting, as

Supplemental Material >

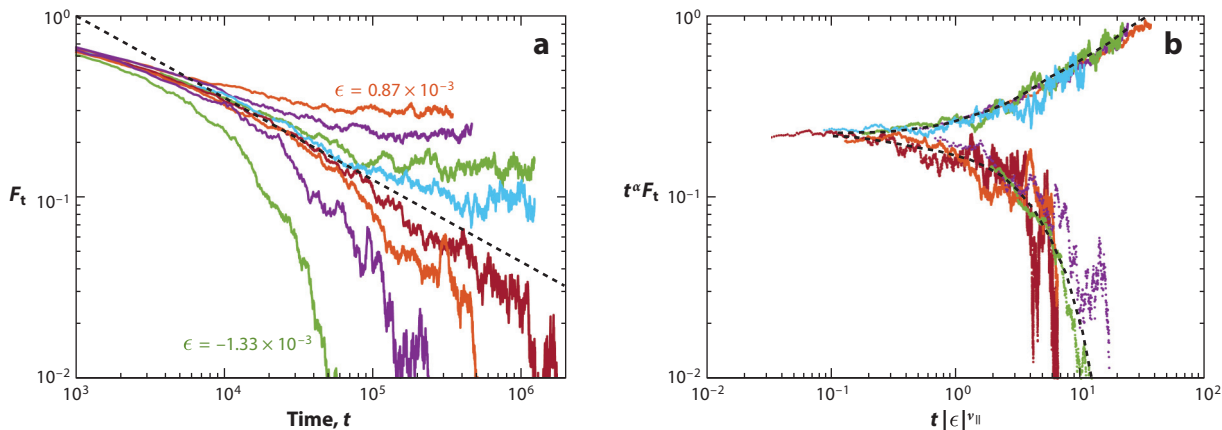


Figure 16

(a) Turbulence fraction F_t as a function of time for a range of Reynolds numbers initialized with uniform turbulence. Above criticality, the turbulence fraction saturates at a finite value, and below it falls to zero. At criticality, the turbulence fraction decays in time as a power law, $F_t \sim t^{-\alpha}$, with the directed percolation exponent $\alpha \simeq 0.4505$ (dashed line). Colored lines from highest to lowest F_t correspond to evolution at reduced Reynolds numbers ranging from $\epsilon = 0.87 \times 10^{-3}$ to $\epsilon = -1.33 \times 10^{-3}$. (b) Data above and below criticality collapse onto two scalings (black dashed curves) when the directed percolation exponents are used to rescale time and the turbulence fraction. All lengths are in units of b ; time, t , is in advective units, b/U , where b and U are respectively the half-gap and velocity of the corresponding plane Couette flow. Figure adapted with permission from Chantry et al. (2017).

in **Figure 6a,c**. The two curves cross at $Re = 325$ (using the conventions of plane Couette flow), which defines a critical point beyond which splitting dominates decay, as pioneered by Avila et al. (2011) for pipe flow. This value should approximate the directed percolation threshold, were such a calculation to be carried out for fully resolved wall-bounded plane Couette flow. Note that this implies that the states with $Re \leq 325$ seen in **Figure 6** are probably long transients. The value of $Re = 323$ was already mentioned by Bottin et al. (1998), although in reference to discontinuous experimental results like those of **Figure 15b**. Lemoult et al. (2016) combined the narrow-gap limit with a drastic reduction in the spanwise direction by reducing the axial height (see **Figure 14**) so that turbulence would take the form of patches rather than bands. They showed that the transition to turbulence for this case verified the scalings of one-dimensional directed percolation.

An important open question is the nature of the transition in plane Poiseuille flow. Sano & Tamai (2016) reported evidence for directed percolation with a critical Reynolds number of $Re_{\text{poi}} = 830$. However, as seen in **Figure 9b**, this transition is preceded by the formation of robust oblique turbulent bands at Reynolds numbers as low as $Re_{\text{poi}} = 660$ (Xiong et al. 2015, Tao et al. 2018). Thus, the transition in plane Poiseuille flow may be more complicated than standard directed percolation.

6. OTHER FLOWS

Oblique turbulent bands form when there is one confined and two extended directions. In addition to the previously mentioned study by Lemoult et al. (2016), several other scenarios have been explored in which the bands become patches or puffs when one of the extended directions is reduced. **Figure 17** shows pressure-driven flows in two parameterized geometries: axially driven flow between two concentric cylinders, called annular pipe flow (Ishida et al. 2016), and flow through a rectangular duct (Takeishi et al. 2015). The analog of the spanwise direction (perpendicular to

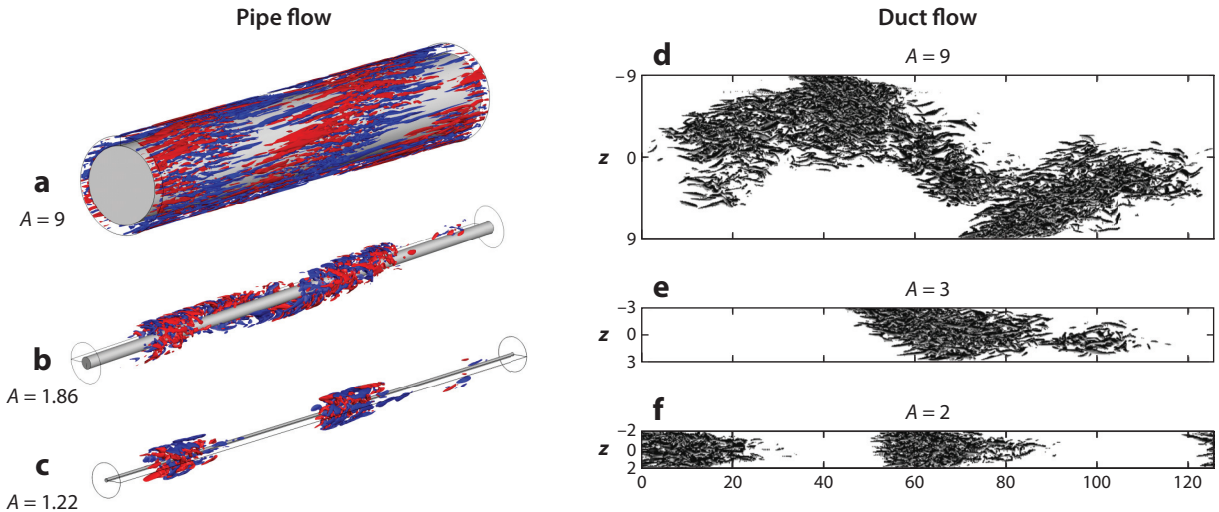


Figure 17

Turbulent–laminar patterns in annular pipe flow (*a–c*) and in duct flow (*d–f*). The aspect ratio A is defined as $A = (r_{\text{out}} + r_{\text{in}})/(r_{\text{out}} - r_{\text{in}})$ for annular pipe flow and as $A = L_{\text{span}}/\text{height}$ for duct flow. For large A , there are two extended directions and turbulence takes the form of oblique bands. For small A , only the streamwise direction is extended and turbulence takes the form of puffs. Lengths in panels *d–f* are in units of the half-height, b . Panels adapted with permission from (*a–c*) Ishida et al. (2016) and (*d–f*) Takeishi et al. (2015).

the gap and to the streamwise direction) is the circumference for the annular pipe and the larger cross-sectional dimension for the duct. For both flows, a spanwise-to-gap aspect ratio A can be defined; both approach plane Poiseuille flow in the limit of infinite aspect ratio and resemble pipe flow in the limit of small aspect ratio. **Figure 17** shows oblique bands for large A and localized puffs for small A .

For counter-rotating Taylor–Couette flow, in which turbulent bands were first discovered, the directions analogous to streamwise and spanwise are azimuthal and axial. An experimental realization by Goharzadeh & Mutabazi (2001) is shown in **Figure 18**, along with a numerical realization by Meseguer et al. (2009) (see also Dong 2009). Rotating plane Couette flow (where the axis of rotation is oriented in the spanwise direction) is closely related to Taylor–Couette flow; this flow has been surveyed, and turbulent bands have been observed by Tsukahara et al. (2010) and Brethouwer et al. (2012). Torsional Couette flow, the flow between two differentially rotating closely spaced disks, is another variant, in which the analog of the streamwise direction is azimuthal, as in Taylor–Couette flow, but the analogs of the spanwise and gap directions are radial and axial. **Figure 18c** shows an experimental realization of spiraling widely spaced turbulent bands in this flow by Cros & Le Gal (2002). An oblique turbulent patch has also been seen in a Poiseuille–Couette experiment with one moving wall and zero mean flux by Klotz et al. (2017), as shown in **Figure 18d**.

Turbulent bands have been sought in other flows, with a view to determining which features favor or suppress them. Brethouwer et al. (2012) observed bands in Couette and Poiseuille flows subjected to stabilizing influences such as stratification, cyclonic rotation, or a magnetic field, but at higher and wider Reynolds number ranges. Spatially localized turbulence was also studied by Zikanov et al. (2014) and Deusebio et al. (2015) in the presence of a magnetic field and stratification, respectively. Wang et al. (2017) observed oblique bands in simulations of viscoelastic turbulence in channel flow. Ishida et al. (2017) found that rough walls tend to suppress turbulent bands in plane Poiseuille flow. Khapko et al. (2016) found that the asymptotic suction boundary

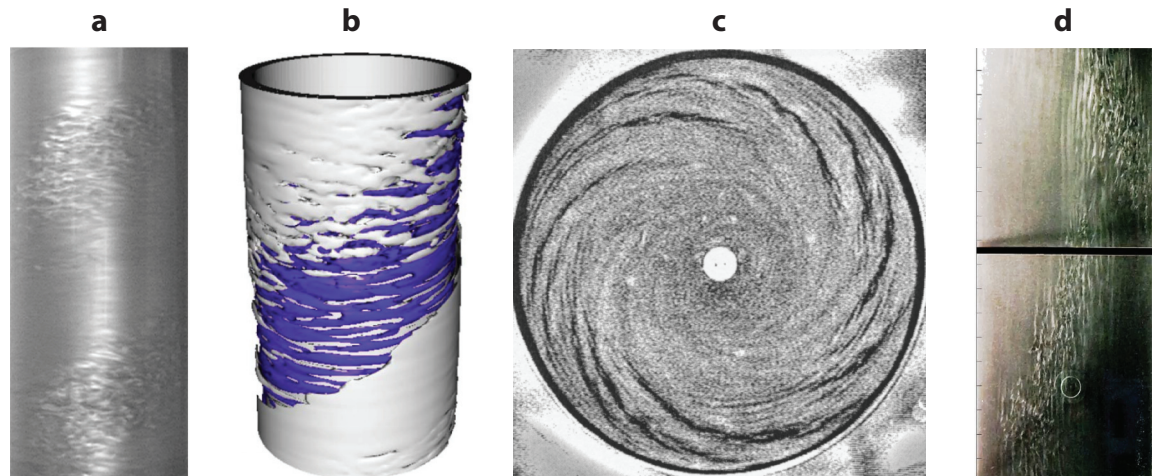


Figure 18

Turbulent bands in a counter-rotating Taylor–Couette experiment (*a*) and simulation (*b*). (*c*) Spiraling turbulent bands in an experiment on torsional Couette flow between closely spaced differentially rotating disks. (*d*) Oblique turbulent patch in a Poiseuille–Couette experiment. Panels adapted with permission from (*a*) Goharzadeh & Mutabazi (2001), (*b*) Meseguer et al. (2009), (*c*) Cros & Le Gal (2002), and (*d*) Klotz et al. (2017).

layer does not support oblique turbulent bands. They provided evidence that this is due to the lack of vertical confinement, more specifically the fact that a boundary layer, bordered by only one wall, allows large-scale wall-normal flows. This is consistent with the analysis of Duguet & Schlatter (2013) on the role of incompressibility of the large-scale flows in generating oblique structures.

7. CONCLUSION

In all of the transitional flows we have depicted, turbulence takes the form of long and well-separated oblique bands. These bands exist whenever the domain is sufficiently large to accommodate them, and this is true even very close to the threshold for turbulence, e.g., in **Figure 6d** or **Figure 14**. Their widths and angles remain comparable to those in a regularly spaced pattern, even when the bands are isolated or sparsely scattered throughout the domain. They occur in the hydrodynamic flows discussed in detail here, i.e., plane Couette flow and Poiseuille flow, and also in many other flows such as Taylor–Couette flow, torsional Couette flow, and annular pipe flow.

A tilted rectangular domain with periodic boundary conditions (MBU) provides the minimal horizontal domain in which one or a few turbulent bands can be computed. By reproducing their phenomenology with free-slip boundary conditions, we have shown that the boundary layers are unimportant and the effect of the walls is only to produce shear and confinement. In order to carry out simulations in domains containing a large number of bands, we have shown that a minimal model of the vertical dependence retains the qualitative properties of transitional plane Couette flow, and we have used this model to show that the transition to turbulence via band extinction is in the universality class of directed percolation.

Turbulent bands assemble and organize the much smaller streamwise streaks and vortices of which they are composed. First considered as an exotic manifestation and generalization of pattern formation, turbulent bands have turned out to be elementary and fundamental components of transitional flows, much like the streaks and vortices. They occupy an intermediate position

in the hierarchy between the large horizontal dimensions of a domain and the vertical gap size that is the scale of the streaks and vortices. The bands exist symbiotically with large-scale flows; the interaction between the two is responsible for maintaining them. Yet, despite the considerable interest and effort devoted to their study, the mechanisms producing the bands remain, at best, incompletely understood. Their angles and widths cannot yet be quantitatively explained by a predictive theory from first principles.

DISCLOSURE STATEMENT

The authors are not aware of any biases that might be perceived as affecting the objectivity of this review.

ACKNOWLEDGMENTS

We thank Yohann Duguet for helpful comments. This work was performed using high-performance computing resources provided by the Institut du Développement et des Ressources en Informatique Scientifique (IDRIS) of the Centre National de la Recherche Scientifique (CNRS), coordinated by GENCI (Grand Equipement National de Calcul Intensif) through a series of grants, including 1119, i20070211119, i20080211119, i2009021119, i2010021119, i2011021119, i2012021119, i20132a1119, i20142a1119, i20152a1119, i20162a1119, and A0022A01119. The authors are grateful for support from the Agence Nationale de la Recherche (ANR) through the TRANSFLOW project. This research was supported in part by the National Science Foundation under grant number NSF PHY-1748958 and by a CNRS/Royal Society grant.

LITERATURE CITED

- Anderreck CD, Liu S, Swinney HL. 1986. Flow regimes in a circular Couette system with independently rotating cylinders. *J. Fluid Mech.* 164:155–83
- Avila K. 2013. *Shear flow experiments: Characterizing the onset of turbulence as a phase transition*. PhD Thesis, Georg August Univ. Sch. Sci., Göttingen, Ger.
- Avila K, Moxey D, de Lozar A, Avila M, Barkley D, Hof B. 2011. The onset of turbulence in pipe flow. *Science* 333:192–96
- Barkley D, Tuckerman LS. 2005a. Computational study of turbulent laminar patterns in Couette flow. *Phys. Rev. Lett.* 94:014502
- Barkley D, Tuckerman LS. 2005b. Turbulent-laminar patterns in plane Couette flow. In *IUTAM Symposium on Laminar-Turbulent Transition and Finite Amplitude Solutions*, ed. T Mullin, R Kerswell, pp. 107–27. Dordrecht, Neth.: Springer
- Barkley D, Tuckerman LS. 2007. Mean flow of turbulent–laminar patterns in plane Couette flow. *J. Fluid Mech.* 576:109–37
- Bottin S, Chaté H. 1998. Statistical analysis of the transition to turbulence in plane Couette flow. *Eur. Phys. J. B* 6:143–55
- Bottin S, Daviaud F, Manneville P, Dauchot O. 1998. Discontinuous transition to spatiotemporal intermittency in plane Couette flow. *Europhys. Lett.* 43:171–76
- Brethouwer G, Duguet Y, Schlatter P. 2012. Turbulent-laminar coexistence in wall flows with Coriolis, buoyancy or Lorentz forces. *J. Fluid Mech.* 704:137–72
- Campbell D, Farmer D, Crutchfield J, Jen E. 1985. Experimental mathematics: the role of computation in nonlinear science. *Commun. ACM* 28:374–84
- Chantry M, Tuckerman LS, Barkley D. 2016. Turbulent–laminar patterns in shear flows without walls. *J. Fluid Mech.* 791:R8

- Chantry M, Tuckerman LS, Barkley D. 2017. Universal continuous transition to turbulence in a planar shear flow. *J. Fluid Mech.* 824:R1
- Coles D, van Atta C. 1966. Progress report on a digital experiment in spiral turbulence. *AIAA J.* 4:1969–71
- Couliou M, Monchoux R. 2015. Large-scale flows in transitional plane Couette flow: a key ingredient of the spot growth mechanism. *Phys. Rev. Fluids* 27:034101
- Couliou M, Monchoux R. 2018. Childhood of turbulent spots in a shear flow. *Phys. Rev. Fluids* 3:123901
- Cros A, Le Gal P. 2002. Spatiotemporal intermittency in the torsional Couette flow between a rotating and a stationary disk. *Phys. Fluids* 14:3755–65
- Cvitanović P, Eckhardt B. 1989. Periodic-orbit quantization of chaotic systems. *Phys. Rev. Lett.* 63:823
- Daviaud F, Hegseth J, Bergé P. 1992. Subcritical transition to turbulence in plane Couette flow. *Phys. Rev. Lett.* 69:2511
- Deguchi K, Hall P. 2015. Asymptotic descriptions of oblique coherent structures in shear flows. *J. Fluid Mech.* 782:356–67
- Deusebio E, Caulfield C, Taylor J. 2015. The intermittency boundary in stratified plane Couette flow. *J. Fluid Mech.* 781:298–329
- Dong S. 2009. Evidence for internal structures of spiral turbulence. *Phys. Rev. E* 80:067301
- Duguet Y, Schlatter P. 2013. Oblique laminar-turbulent interfaces in plane shear flows. *Phys. Rev. Lett.* 110:034502
- Duguet Y, Schlatter P, Henningson DS. 2010. Formation of turbulent patterns near the onset of transition in plane Couette flow. *J. Fluid Mech.* 650:119–29
- Feynman RP. 1964. *Lecture Notes in Physics*. Reading, MA: Addison-Wesley
- Fukudome K, Iida O. 2012. Large-scale flow structure in turbulent Poiseuille flows at low-Reynolds numbers. *J. Fluid Sci. Technol.* 7:181–95
- Gibson JF, Halcrow J, Cvitanović P. 2009. Equilibrium and travelling-wave solutions of plane Couette flow. *J. Fluid Mech.* 638:243–66
- Goharzadeh A, Mutabazi I. 2001. Experimental characterization of intermittency regimes in the Couette-Taylor system. *Eur. Phys. J. B* 19:157–62
- Goharzadeh A, Mutabazi I. 2008. The phase dynamics of spiral turbulence in the Couette-Taylor system. *Eur. Phys. J. B* 66:81–84
- Hamilton JM, Kim J, Waleffe F. 1995. Regeneration mechanisms of near-wall turbulence structures. *J. Fluid Mech.* 287:317–48
- Hashimoto S, Hasobe A, Tsukahara T, Kawaguchi Y, Kawamura H. 2009. An experimental study on turbulent-stripe structure in transitional channel flow. In *Proceedings of the Sixth International Symposium on Turbulence, Heat and Mass Transfer*, ed. K Hanjalić, Y Nagano, S Jakirlić. Danbury, CT: Begell House
- Hegseth JJ, Andereck CD, Hayot F, Pomeau Y. 1989. Spiral turbulence and phase dynamics. *Phys. Rev. Lett.* 62:257
- Henderson RD, Karniadakis GE. 1995. Unstructured spectral element methods for simulation of turbulent flows. *J. Comput. Phys.* 122:191–217
- Ishida T, Brethouwer G, Duguet Y, Tsukahara T. 2017. Laminar-turbulent patterns with rough walls. *Phys. Rev. Fluids* 2:073901
- Ishida T, Duguet Y, Tsukahara T. 2016. Transitional structures in annular Poiseuille flow depending on radius ratio. *J. Fluid Mech.* 794:R2
- Kanazawa T. 2018. *Lifetime and growing process of localized turbulence in plane channel flow*. PhD Thesis, Osaka Univ., Osaka, Jpn.
- Kawahara G, Kida S. 2001. Periodic motion embedded in plane Couette turbulence: regeneration cycle and burst. *J. Fluid Mech.* 449:291–300
- Kawahara G, Uhlmann M, Van Veen L. 2012. The significance of simple invariant solutions in turbulent flows. *Annu. Rev. Fluid Mech.* 44:203–25
- Khapko T, Schlatter P, Duguet Y, Henningson D. 2016. Turbulence collapse in a suction boundary layer. *J. Fluid Mech.* 795:356–79
- Klotz L, Lemoult G, Frontczak I, Tuckerman LS, Wesfreid JE. 2017. Couette-Poiseuille flow experiment with zero mean advection velocity: subcritical transition to turbulence. *Phys. Rev. Fluids* 2:043904

- Kushwaha A, Park JS, Graham MD. 2017. Temporal and spatial intermittencies within channel flow turbulence near transition. *Phys. Rev. Fluids* 2:024603
- Lagha M, Manneville P. 2007. Modeling of plane Couette flow. I. Large scale flow around turbulent spots. *Phys. Fluids* 19:094105
- Lemoult G, Gumowski K, Aider JL, Wesfreid JE. 2014. Turbulent spots in channel flow: an experimental study. *Eur. Phys. J. E* 37:25
- Lemoult G, Shi L, Avila K, Jalikop SV, Avila M, Hof B. 2016. Directed percolation phase transition to sustained turbulence in Couette flow. *Nat. Phys.* 12:254–58
- Lübeck S. 2004. Universal scaling behavior of non-equilibrium phase transitions. *Int. J. Mod. Phys. B* 18:3977–4118
- Lundbladh A, Johansson AV. 1991. Direct simulation of turbulent spots in plane Couette flow. *J. Fluid Mech.* 229:499–516
- Manneville P. 2015. On the transition to turbulence of wall-bounded flows in general, and plane Couette flow in particular. *Eur. J. Mech. B* 49:345–62
- Manneville P, Dauchot O. 2001. Patterning and transition to turbulence in subcritical systems: the case of plane Couette flow. In *Coherent Structures in Complex Systems: Selected Papers of the XVII Sitges Conference on Statistical Mechanics*, ed. D Reguera, LL Bonilla, JM Rubi, pp. 58–79. Berlin: Springer
- Manneville P, Locher F. 2000. A model for transitional plane Couette flow. *C.R. Acad. Sci. Paris III* 328:159–64
- Marqués F. 1990. On boundary conditions for velocity potentials in confined flows: application to Couette flow. *Phys. Fluids A* 2:729–37
- Meseguer A, Mellibovsky F, Avila M, Marques F. 2009. Instability mechanisms and transition scenarios of spiral turbulence in Taylor–Couette flow. *Phys. Rev. E* 80:046315
- Mizuno Y, Jiménez J. 2013. Wall turbulence without walls. *J. Fluid Mech.* 723:429–55
- Moehlis J, Faisst H, Eckhardt B. 2004. A low-dimensional model for turbulent shear flows. *New J. Phys.* 6:56
- Nagata M. 1990. Three-dimensional finite-amplitude solutions in plane Couette flow: bifurcation from infinity. *J. Fluid Mech.* 217:519–27
- Philip J, Manneville P. 2011. From temporal to spatiotemporal dynamics in transitional plane Couette flow. *Phys. Rev. E* 83:036308
- Podvin B, Fraigneau Y. 2011. Synthetic wall boundary conditions for the direct numerical simulation of wall-bounded turbulence. *J. Turbul.* 12:N4
- Pomeau Y. 1986. Front motion, metastability and subcritical bifurcations in hydrodynamics. *Physica D* 23:3–11
- Prigent A, Grégoire G, Chaté H, Dauchot O. 2003. Long-wavelength modulation of turbulent shear flows. *Physica D* 174:100–13
- Prigent A, Grégoire G, Chaté H, Dauchot O, van Saarloos W. 2002. Large-scale finite-wavelength modulation within turbulent shear flows. *Phys. Rev. Lett.* 89:014501
- Reetz F, Kreilos T, Schneider TM. 2019. Exact invariant solution reveals the origin of self-organized oblique turbulent-laminar stripes. *Nat. Commun.* 10:2277
- Sano M, Tamai K. 2016. A universal transition to turbulence in channel flow. *Nat. Phys.* 12:249–53
- Schneider TM, Marinc D, Eckhardt B. 2010. Localized edge states nucleate turbulence in extended plane Couette cells. *J. Fluid Mech.* 646:441–51
- Schumacher J, Eckhardt B. 2001. Evolution of turbulent spots in a parallel shear flow. *Phys. Rev. E* 63:046307
- Seshasayanan K, Manneville P. 2015. Laminar-turbulent patterning in wall-bounded shear flows: a Galerkin model. *Fluid Dyn. Res.* 47:035512
- Shi L, Avila M, Hof B. 2013. Scale invariance at the onset of turbulence in Couette flow. *Phys. Rev. Lett.* 110:204502
- Takeishi K, Kawahara G, Wakabayashi H, Uhlmann M, Pinelli A. 2015. Localized turbulence structures in transitional rectangular-duct flow. *J. Fluid Mech.* 782:368–79
- Tao J, Eckhardt B, Xiong X. 2018. Extended localized structures and the onset of turbulence in channel flow. *Phys. Rev. Fluids* 3:011902
- Tillmark N, Alfredsson PH. 1992. Experiments on transition in plane Couette flow. *J. Fluid Mech.* 235:89–102

- Tsukahara T, Iwamoto K, Kawamura H, Takeda T. 2006. DNS of heat transfer in a transitional channel flow accompanied by a turbulent puff-like structure. In *Proceedings of the Fifth International Symposium on Turbulence, Heat and Mass Transfer*, ed. K Hanjalić, Y Nagano, S Jakirlić, pp. 193–96. Danbury, CT: Begell House
- Tsukahara T, Seki Y, Kawamura H, Tochio D. 2005. DNS of turbulent channel flow at very low Reynolds numbers. In *Proceedings of the Fourth International Symposium on Turbulence and Shear Flow Phenomena*, pp. 935–40. Danbury, CT: Begell House
- Tsukahara T, Tillmark N, Alfredsson P. 2010. Flow regimes in a plane Couette flow with system rotation. *J. Fluid Mech.* 648:5–33
- Tuckerman LS, Barkley D. 2011. Patterns and dynamics in transitional plane Couette flow. *Phys. Fluids* 23:041301
- Tuckerman LS, Kreilos T, Schrobsdorff H, Schneider TM, Gibson JF. 2014. Turbulent-laminar patterns in plane Poiseuille flow. *Phys. Fluids* 26:114103
- Waleffe F. 1997. On a self-sustaining process in shear flows. *Phys. Fluids* 9:883–90
- Wang SN, Shekar A, Graham MD. 2017. Spatiotemporal dynamics of viscoelastic turbulence in transitional channel flow. *J. Non-Newton. Fluid Mech.* 244:104–22
- Xiong X, Tao J, Chen S, Brandt L. 2015. Turbulent bands in plane-Poiseuille flow at moderate Reynolds numbers. *Phys. Fluids* 27:041702
- Zikanov O, Krasnov D, Boeck T, Thess A, Rossi M. 2014. Laminar-turbulent transition in magnetohydrodynamic duct, pipe, and channel flows. *Appl. Mech. Rev.* 66:030802